hydrolysis. Of the several simple amines that were tried with copper(II), 2,2′-bipyridine gave the most satisfactory combination of high hydrolysis rates and catalyst longevity. Bipyridine complexes of Cu(II) may be better catalysts for phosphate ester hydrolysis because of a favorable change in the equilibrium constant for coordination to anionic ligands promoted by the π acidity of 2,2′-bipyridine[54] or by some favorable effect in the decomposition of **5** to products.

Conclusions

These studies show that one can develop long-lived transition-metal catalysts for the hydrolysis of phosphate diesters in aqueous solution near neutral pH. The mechanism of catalysis includes substrate binding to the metal hydroxide complex, followed by intramolecular attack of hydroxide on phosphate ester, and P–O bond cleavage. The cationic metal catalyst effectively neutralizes the electrostatic barrier to hydroxide nucleophilic attack on phosphate diesters and monoesters; these anionic esters are hydrolyzed only 60-fold more slowly than the neutral phosphate triester. Of the first-row divalent transition-metal cations surveyed, Ni^{2+} and Cu^{2+} having high catalytic activity may reflect a favorable binding that occurs reversibly for these softer metals and a low pK_a for coordinated water. Metal-ion-catalyzed hydrolysis of phosphate diesters could play a role in DNA damage by transition-metal ions, as well as in the development of footprinting reagents. Further studies along these lines are under way.

Acknowledgment. This research was supported by the Army Research Office (Grant DAAG29-85-KO263). We thank Marco Lopez, Charles Perrin, and Frank Westheimer for helpful discussions and Bruce Dyke for calculation of concentrations of copper 2,2′-bipyridine complexes.

Supplementary Material Available: Tables of kinetic data for hydrolysis of phosphate esters by $Cu(bpy)^{2+}$ (6 pages). Ordering information is given on any current masthead page.

(54) Sigel, H. *Angew. Chem., Int. Ed. Engl.* **1975**, *14*, 394-402.

Contribution from the Department of Chemistry,
The University of Michigan, Ann Arbor, Michigan 48109-1055

Dimeric Complexes Containing the $[Fe_2S_2]^{2+}$ Cores Coordinated by Non-Sulfur Terminal Ligands.[1] Synthesis, Structural Characterization, and Spectroscopic Properties of $[Et_4N]_2[Fe_2S_2(o,o'\text{-}C_{12}H_8O_2)_2]$, $[Et_4N]_2[Fe_2S_2(C_4H_4N)_4]$, and $[Et_4N]_2[Fe_2S_2(O\text{-}o\text{-}C_6H_4CH(n\text{-}C_4H_9)NHC_6H_4\text{-}o\text{-}S)_2]$ and the Structure of $[Ph_4P]_2[Fe_2S_2(OC_6H_4\text{-}p\text{-}CH_3)_4]$

A. Salifoglou, A. Simopoulos,[2] A. Kostikas,[2] R. W. Dunham,[3] M. G. Kanatzidis, and D. Coucouvanis*

Received January 28, 1988

The synthesis and spectroscopic characterization of the $[Fe_2S_2L_4]^{2-}$ clusters (L_2 = $o,o'\text{-}C_{12}H_8O_2^{2-}$, $^-O\text{-}o\text{-}C_6H_4CH(n\text{-}Bu)NHC_6H_4\text{-}o\text{-}S^-$; L = $^-OC_6H_4\text{-}p\text{-}CH_3$, $C_4H_4N^-$) are reported. The crystal and molecular structures of $(Et_4N)_2[Fe_2S_2(o,o'\text{-}C_{12}H_8O_2)_2]$ (I), $(Et_4N)_2[Fe_2S_2(C_4H_4N)_4]$ (II), $(Et_4N)_2[Fe_2S_2(O\text{-}o\text{-}C_6H_4CH(n\text{-}Bu)NHC_6H_4\text{-}o\text{-}S)_2]$ (III), and $(Ph_4P)_2[Fe_2S_2(OC_6H_4\text{-}p\text{-}CH_3)_4]$ (IV) are described in detail. I crystallizes in the monoclinic space group $C2/c$, with cell dimensions a = 11.500 (2) Å, b = 13.541 (3) Å, c = 26.612 (5) Å, β = 92.25 (1)°, and Z = 4. II crystallizes in monoclinic space group $P2_1/n$, with cell dimensions a = 9.689 (3) Å, b = 16.362 (2) Å, c = 11.910 (5) Å, β = 97.74 (3)°, and Z = 2. III crystallizes in the monoclinic space group $P2_1/c$, with cell dimensions a = 14.878 (4) Å, b = 9.585 (3) Å, c = 18.950 (6) Å, β = 95.59 (2)°, and Z = 2, and IV crystallizes in the monoclinic space group $P2_1/a$, with cell dimensions a = 16.308 (5) Å, b = 16.674 (6) Å, c = 24.456 (9) Å, β = 91.13 (3)°, and Z = 4. Intensity data for I–IV were collected on a four-circle computer-controlled diffractometer with use of the θ–2θ scan technique. All four structures were solved by conventional methods from 2739, 1736, 2086 and 3632 reflections for I–IV, respectively. The structures were refined by full-matrix least-squares techniques (310 parameters for I, 173 parameters for II, 280 parameters for III, and 385 parameters for IV) to final R values of 0.033 (I), 0.069 (II), 0.065 (III), and 0.074 (IV). Complexes I–IV contain the planar $[Fe_2S_2]^{2+}$ cores coordinated fully or partially by non-sulfur terminal ligands. The Fe···Fe distance in the centrosymmetric dianions ranges from 2.677 (3) Å in II to 2.749 (24) Å in IV. The Fe–O distances are 1.894 (2) (I), 1.921 (11) (III), and 1.870 (12) Å (IV), and the $\overline{Fe\text{–}N}$ distance in II is 1.97 (5) Å. Structural comparisons with the already reported thiolate dimers $[Fe_2S_2L_4]^{2-}$ (L = ^-SAr; L_2 = $S_2\text{-}o\text{-}xyl^{2-}$) are reported. The electronic, Mössbauer, cyclic voltammetric, and proton magnetic resonance properties of the new dimers are discussed in detail. A comparison of these properties with the available data on the Rieske $[Fe_2S_2]$ centers is presented and certain conclusions are drawn concerning future design of synthetic analogues.

Introduction

A detailed understanding of the metal centers in the plant type two iron ferredoxins[4] was greatly facilitated by the isolation and structural characterization of several synthetic analogue complexes with the general formula $[L_2FeS_2FeL_2]^{2-}$ (L_2 = o-xylene-α,α'-dithiolate;[5] L = $^-S\text{-}C_6H_4\text{-}p\text{-}CH_3$,[5] Cl^-,[5b] L_2 = S_5^{2-}[6]). Detailed comparative studies of the Mossbauer, electron paramagnetic resonance (EPR), and electronic spectra of the dimeric analogue complexes[7] and of representative 2Fe-2S ferredoxins led[8] to the realization that the iron–sulfur cores in the latter were structurally identical with the planar rhombic Fe_2S_2 units in the former. The

(1) Coucouvanis, D.; Salifoglou, A.; Kanatzidis, M. G.; Simopoulos, A.; Papaefthymiou, V. *J. Am. Chem. Soc.* **1984**, *106*, 6081.
(2) Nuclear Research Center, "Demokritos", Aghia Paraskevi, Attiki, Greece.
(3) The Biophysics Research Division and the Department of Biological Chemistry, The University of Michigan, Ann Arbor, MI 48109.
(4) (a) Orme-Johnson, W. H. *Annu. Rev. Biochem.* **1973**, *42*, 159. (b) Kimura, T. *Struct. Bonding (Berlin)* **1968**, *5*, 1. (c) Brintzinger, H.; Palmer, G.; Sands, R. H. *Proc. Natl. Acad. Sci. U.S.A.* **1966**, *55*, 397. (d) Gibson, J. F.; Hall, D. O.; Thornley, J. H. M.; Whatley, F. R. *Proc. Natl. Acad. Sci. U.S.A.* **1966**, *56*, 987. (e) Dunham, W. R.; Palmer, G.; Sands, R. H.; Bearden, A. J. *Biochim. Biophys. Acta* **1971**, *253*, 373.
(5) (a) Mayerle, J. J.; Denmark, S. E.; DePamphillis, B. V.; Ibers, J. A.; Holm, R. H. *J. Am. Chem. Soc.* **1975**, *97*, 1032. (b) Wong, G. B.; Bobrick, M. A.; Holm, R. H. *Inorg. Chem.* **1978**, *17*, 578.
(6) Coucouvanis, D.; Swenson, D.; Stremple, P.; Baenziger, N. C. *J. Am. Chem. Soc.* **1979**, *101*, 3392.
(7) (a) Holm, R. H.; Ibers, J. A. In *Iron Sulfur Proteins*; Lovenberg, W., Ed.; Academic: New York, 1977; Vol. 3, Chapter 7 and references therein. (b) Berg, J. M.; Holm, R. H. In *Iron Sulfur Proteins*; Spiro, T. G., Ed.; Wiley-Interscience: New York, 1982; Chapter 1.
(8) Palmer, G. In *Iron Sulfur Proteins*; Lovenberg, W., Ed.; Academic: New York, 1973; Vol. 2, pp 285-325.

0020-1669/88/1327-3394$01.50/0

validity of this structural assignment was confirmed by the X-ray crystal structure determination of the 2Fe-2S ferredoxin from *Spirulina platensis*,[9] which revealed the Fe_2S_2 rhombic unit coordinated by four cysteinyl residues.

A distinct class of [2Fe-2S] proteins with unique properties has been identified in the mitochondrial bc_1 complex and the photosynthetic cytochrome b_6f complex[10] and are referred to as the Rieske proteins.[11] Among the characteristic features that differentiate the Rieske proteins from the conventional [2Fe-2S] ferredoxins, the following are included: (a) a 400–600-mV positive shift in reduction potential; (b) a large inequivalence for the two Fe^{3+} ions in the oxidized form, indicated by the isomer shifts and quadrupole splittings in the ^{57}Fe Mössbauer spectra; (c) a smaller value of the EPR g_{av} for the reduced $[Fe_2S_2]^+$ centers ($\sim$1.85), by comparison to corresponding values typically observed in the reduced [2Fe-2S] ferredoxins ($\sim$1.94); (d) electronic absorption spectra bathochromically shifted by comparison to those of the plant type ferredoxins. These differences very likely have their origin in a major difference in terminal ligand coordination to the $[Fe_2S_2]$ units between the Rieske proteins and the conventional [2Fe-2S] ferredoxins. In the latter, the Fe_2S_2 clusters are bound to the protein by a full complement (four) of cysteinyl sulfur atoms. In contrast, the Fe_2S_2 clusters in the Rieske proteins are bound to the protein matrix by only two cysteinyl residues.[12] The nature of the remaining terminal ligands is only partially established. An ENDOR study[13] has shown the presence of Fe–N bonds, but it has not given evidence regarding the number of nitrogenous ligands (histidine imidazoles?). The question of the distribution of the non-sulfur terminal ligands has remained unanswered until recently. In a study of the resonance Raman spectra of the Rieske proteins from two different sources, evidence has been presented[14] that supports an asymmetric distribution of the Cys, nitrogen, and possibly other (oxygen?) ligands. A recent analysis of the Fe extended X-ray absorption fine structure (EXAFS), in both the oxidized and reduced forms of the Rieske center in *Pseudomonas cepacia* phthalate oxygenase also has revealed the presence of light atoms in the first coordination sphere of the iron atoms together with sulfur atoms.[15]

The apparent need for synthetic Fe_2S_2 analogue complexes, with either mixed (S, X) or non-sulfur (X, X = O, N) terminally coordinated ligands, has stimulated recent synthetic studies in this area. In addition to the $[Fe_2S_2(o,o'\text{-}C_{12}H_8O_2)_2]^{2-}$ and $[Fe_2S_2(C_4H_4N)_4]^{2-}$ anions that have been synthesized and structurally characterized as Et_4N^+ salts,[1] the synthesis and spectroscopic characterization of the $[Fe_2S_2(OPh)_4]^{2-}$[16,17] and $[Fe_2S_2(L)_4]^{2-}$ anions[18] (L_2 = 2-mercaptobenzoate, 2-(mercaptomethyl)benzoate, and (2-mercaptophenyl)acetate) and the spectroscopic characteristics of the $[Fe_2S_2(L)_4]^{3-}$ anions, generated in solution,[17,18] have been reported. In this paper, we report in detail on the synthesis, structural characterization, and spectroscopic properties of $[Et_4N]_2[Fe_2S_2(o,o'\text{-}C_{12}H_8O_2)_2]$ (I), $[Et_4N]_2[Fe_2S_2(C_4H_4N)_4]$ (II), and $[Et_4N]_2[Fe_2S_2(O\text{-}o\text{-}C_6H_4CH(n\text{-}C_4H_9)NHC_6H_4\text{-}o\text{-}S)_2]$ (III) and the molecular structure of the $[Ph_4P]^+$ salt of the previously synthesized and spectroscopically characterized[16,1] $[Fe_2S_2(OC_6H_4\text{-}p\text{-}CH_3)_4]^{2-}$ anion (IV).

Experimental Section

General Procedures. All iron sulfur complexes were prepared in an inert atmosphere by using a Vacuum Atmospheres Dri-lab glovebox filled with prepurified (Matheson) nitrogen gas. The $[Fe_2S_2(C_4H_4N)_4]^{2-}$ complex was handled in Schlenk glassware on a dual-manifold Schlenk line with prepurified nitrogen used as the inert gas.

The chemicals in this research were used as purchased. The solvents acetonitrile (CH_3CN) and diethyl ether ($(C_2H_5)_2O$) were distilled from calcium hydride (CaH_2) under nitrogen after being refluxed for 12 h. The preparation of $[Fe_2S_2(C_4H_4N)_4]^{2-}$ requires rigorously purified tetrahydrofuran (THF), which was obtained by refluxing it with sodium benzophenone overnight, followed by distillation under a nitrogen atmosphere. A 2.5 M solution of *n*-BuLi in hexanes was purchased from Alfa Chemicals. The *o,o'*-biphenol ($HO\text{-}o\text{-}C_6H_4C_6H_4\text{-}o\text{-}OH$) and cresols HOAr (Ar = $C_6H_4\text{-}p\text{-}CH_3$, $C_6H_4\text{-}m\text{-}CH_3$) were purchased from Aldrich. Disodium biphenolate ($NaO\text{-}o\text{-}C_6H_4\text{-}o\text{-}ONa$) and sodium cresolates NaOAr were obtained by the reaction of the corresponding phenol(s) with sodium metal in tetrahydrofuran or diethyl ether under a nitrogen atmosphere. Benzoyl chloride (C_6H_5COCl) was purchased from Aldrich. Commercial grade methylene chloride purchased from Aldrich was distilled from calcium hydride (CaH_2) before use. Dimethylformamide (DMF), also purchased from Aldrich, was stored over 4A Linde molecular sieves for 2 days and then distilled under reduced pressure at 35–40 °C.

Elemental analyses, on samples dried under vacuum for 12 h, were performed by Galbraith Analytical Laboratories, Knoxville, TN, and Spang Microanalytical Laboratory, Eagle Harbor, MI.

Physical Methods. Visible and ultraviolet spectra were recorded on a Varian Cary 219 spectrophotometer. Proton NMR spectra were obtained on a Bruker 360 MHz Fourier transform (FT) NMR spectrometer with a superconducting magnet. The variable-temperature proton NMR spectra were recorded on a Bruker 300-MHz pulse Fourier transform NMR spectrometer. Tetramethylsilane ($(CH_3)_4Si$) was used as an internal standard. Chemical shifts are reported in parts per million (ppm). The following convention is used whenever isotropically shifted NMR spectra are reported. A positive sign is assigned to a resonance appearing downfield from $(CH_3)_4Si$. A negative sign is given to resonances occurring upfield from $(CH_3)_4Si$.

Cyclic voltammetric measurements were performed on a Princeton Applied Research Model 175 universal programmer. The chosen electrochemical cell had platinum working and auxiliary electrodes. As reference electrode, a saturated calomel electrode was used. All solvents used in the electrochemical measurements were properly dried and distilled. The supporting electrolyte used was tetra-*n*-butylammonium perchlorate ($(C_4H_9)_4NClO_4$). Normal concentrations used were 0.001 M in electroanalyte and 0.1 M in supporting electrolyte. Purified argon was used to purge the solutions prior to the electrochemical measurements.

The X-ray powder diffraction patterns were obtained on an Enraf-Nonius power generator using a 114-mm-diameter Debye–Scherrer type camera (Charles Supper Co.) with Ni-filtered copper Cu Kα radiation (λ = 1.5418 Å).

Mössbauer spectra of $[(C_2H_5)_4N]_2[Fe_2S_2(o,o'\text{-}C_{12}H_8O_2)_2]$ and $[(C_2H_5)_4N]_2[Fe_2S_2(C_4H_4N)_4]$ were measured at liquid-nitrogen temperature with a constant acceleration spectrometer. The source was 50 mCi ^{57}Co(Rh) at room temperature. Mössbauer spectra for $[Et_4N]_2[Fe_2S_2(O\text{-}o\text{-}C_6H_4CH(n\text{-}Bu)NHC_6H_4\text{-}o\text{-}S)_2]$ were recorded at 125 K.

Synthesis. Bis(tetraethylammonium) Bis[(*o*,*o'*-biphenolato)(μ-sulfido)ferrate(III)], $[(C_2H_5)_4N]_2[Fe_2S_2(o,o'\text{-}C_{12}H_8O_2)_2]$. A 0.30-g (0.52-mmol) sample of $[(C_2H_5)_4N]_2[Fe_2S_2Cl_4]$[19] was dissolved in about 40 mL of CH_3CN. To this solution was added 0.24 g (1.04 mmol) of solid $NaO\text{-}o\text{-}C_6H_4C_6H_4\text{-}o\text{-}ONa$ under continuous stirring. The resulting reaction mixture was stirred at room temperature for ca. 8–10 min. Immediate color change to bright orange-red occurred upon mixing. The reaction mixture was filtered to remove NaCl. To the filtrate was slowly

(9) (a) Fukuyama, K.; Hase, T.; Matsumoto, S.; Tsukihara, T.; Katsube, Y.; Tanaka, N.; Kakudo, M.; Wada, K.; Matsubara, H. *Nature (London)* **1980**, *286*, 522. (b) Tsukihara, T.; Fukuyama, K.; Nakamura, M.; Katsube, Y.; Tanaka, N.; Kakudo, M.; Wada, K.; Hase, T.; Matsubara, H. *J. Biochem. (Tokyo)* **1982**, *90*, 1763.

(10) (a) Trumpower, L. B.; Katki, A. G. In *Membrane Proteins in Energy Transduction*; Capaldi, R. A., Ed.; Dekker: New York, 1979; pp 89–200. (b) Nelson, N.; Neuman, J. *J. Biol. Chem.* **1972**, *247*, 1817. (c) Hurt, E.; Hauska, G. *Eur. J. Biochem.* **1981**, *117*, 591. (d) Bowyer, T. R.; Crofts, A. R. *Biochim. Biophys. Acta* **1981**, *636*, 218. (e) Gabellini, N.; Bowyer, J. A.; Hurt, E.; Melandri, B. A.; Hauska, G. *Eur. J. Biochem.* **1982**, *126*, 105.

(11) (a) Rieske, J. S.; MacLennan, D. H.; Coleman, R. *Biochem. Biophys. Res. Commun.* **1964**, *15*, 338. (b) Following the first successful purification of this type of 2Fe-2S protein by Rieske et al., this class of ferredoxins is now referred to as the "Rieske proteins".

(12) Fee, J. A.; Findling, K. L.; Yoshida, T.; Hille, R.; Tarr, G. E.; Hearshen, D. O.; Dunham, W. R.; Day, E. P.; Kent, T. A.; Munck, E. *J. Biol. Chem.* **1984**, *259*, 124.

(13) Cline, J. F.; Hoffman, B. M.; Mims, W. B.; LaHaie, E.; Ballou, D. P.; Fee, J. A. *J. Biol. Chem.* **1985**, *260*, 3251.

(14) Kuila, D.; Fee, J. A.; Schoonover, J. R.; Woodruff, W. H.; Batie, C. J.; Ballou, D. P. *J. Am. Chem. Soc.* **1987**, *109*, 1559.

(15) Penner-Hahn, J. E.; Tsang, H. T.; Batie, C. J.; Ballou, D. P. *Recl.: J. R. Neth. Chem. Soc.* **1987**, *106*(6–7), 228.

(16) Cleland, W. E.; Averill, B. A. *Inorg. Chem.* **1984**, *23*, 4192.

(17) Beardwood, P.; Gibson, J. F. *J. Chem. Soc., Chem. Commun.* **1985**, 102.

(18) (a) Beardwood, P.; Gibson, J. F. *J. Chem. Soc., Chem. Commun.* **1986**, 490. (b) Beardwood, P.; Gibson, J. F. *J. Chem. Soc., Chem. Commun.* **1985**, 1345.

(19) Bobrik, M. A.; Hodgson, K. O.; Holm, R. H. *Inorg. Chem.* **1977**, *16*, 1851.

added 80–100 mL of diethyl ether. When this was allowed to stand overnight, orange-red crystals were deposited and were isolated by filtration, washed twice with diethyl ether, and dried under vacuum. Analytically pure product was obtained by recrystallization of the crude crystalline material from a mixture of $CH_3CN/(C_2H_5)_2O$. Yield: 0.33 g (79.1%).

Anal. Calcd for $Fe_2S_2O_4N_2C_{40}H_{56}$ (mol wt 804): C, 59.70; H, 6.97; N, 3.48; Fe, 13.93; S, 7.96. Found: C, 58.48; H, 6.96; N, 3.49; Fe, 12.84; S, 8.08.

Electronic absorption spectrum (CH_3CN solution), λ_{max} (nm) (ϵ_m): 295 (31 680), 416 (9265), 485 (sh ~5445), 522 (sh ~3920).

Bis(tetraphenylphosphonium) Bis[(*o*,*o*′-biphenolato)(μ-sulfido)ferrate(III)], $[(C_6H_5)_4P]_2[Fe_2S_2(o,o'\text{-}C_{12}H_8O_2)_2]$. The tetraphenyl phosphonium salt was prepared by a procedure identical with that used to prepare the tetraethylammonium salt. The reactants as well as their quantities used in the reaction were as follows: 0.22 g (0.22 mmol) of $[(C_6H_5)_4P]_2[Fe_2S_2Cl_4]$ and 0.10 g (0.43 mmol) of NaO-*o*-$C_6H_4C_6H_4$-*o*-ONa in 40 mL of CH_3CN. When the mixture was allowed to stand overnight, orange-red microcrystalline material precipitated out of solution. The product was isolated by filtration, washed twice with diethyl ether, and dried under vacuum. Recrystallization of the crude material from a mixture of $CH_3CN/(C_2H_5)_2O$ afforded 0.12 g of orange-red crystalline product. Yield: 44.5%.

Anal. Calcd for $Fe_2S_2O_4P_2C_{72}H_{56}$ (mol wt 1222): C, 70.70; H, 4.58. Found: C, 68.58; H, 4.32.

The electronic spectrum of this derivative was virtually identical with that of the Et_4N^+ analogue.

Observed powder pattern (2θ values; λ(Cu Kα) = 1.5418 Å; the first 19 lines): 7.08 (vs), 9.68 (s), 10.43 (w), 11.93 (w), 12.65 (m), 13.50 (s), 15.03 (vw), 16.75 (vw), 17.98 (s), 19.40 (vw), 20.23 (m), 20.95 (w) 21.63 (m), 22.60 (w), 23.45 (s), 24.18 (w), 24.98 (m), 25.90 (w), 26.58 (w).

Bis(tetraethylammonium) Bis[bis(pyrrolato)(μ-sulfido)ferrate(III)], $[(C_2H_5)_4N]_2[Fe_2S_2(C_4H_4N)_4]$. A 0.35-g (0.60-mmol) sample of $[(C_2H_5)_4N]_2[Fe_2S_2Cl_4]$ was dissolved in about 40 mL of CH_3CN. In a 50-mL round-bottom flask, 0.16 g (2.40 mmol) of pyrrole was dissolved in 10 mL of freshly distilled tetrahydrofuran. To that was added 0.16 g (2.49 mmol) (0.937 mL) of a 2.5 M BuLi solution in hexanes dropwise with a syringe under continuous stirring. The resulting colorless to pale yellow solution was stirred briefly and then introduced to the $[Fe_2S_2Cl_4]^{2-}$ solution in very small portions—by using a cannula—under continuous stirring. Immediate color change to deep red occurred upon mixing. The resulting reaction mixture was stirred at room temperature for ca. 10–15 min. Then it was filtered, and to the filtrate was added 100 mL of diethyl ether. When this was allowed to stand for 24 h, pure dark red crystals were obtained. The crystals were isolated by filtration, washed with two 10 mL portions of diethyl ether, and dried under vacuum. Yield: 0.30 g (70.8%). The product can be recrystallized from CH_3CN–diethyl ether mixtures. Pure product may also be obtained by repeated dissolution of the crude product and removal of the CH_3CN solvent under vacuum.

Anal. Calcd for $Fe_2S_2N_6C_{32}H_{56}$ (mol wt 700): C, 54.85; H, 8.00; N, 12.00; Fe, 16.00; S, 9.14. Found: C, 51.70; H, 8.35; N, 10.91; Fe, 15.67; S, 9.83.

Electronic absorption spectrum (CH_3CN solution), λ_{max} (nm) (ϵ_m): 370 (8330), 490 (sh, 3290), 550 (sh, 2480).

Calculated powder pattern (2θ values; λ(Cu Kα) = 1.5418 Å; the first 20 lines, with the relative intensities normalized to 100): 9.235 (100.0), 10.715 (92), 12.635 (30), 13.763 (29), 15.015 (9), 15.501 (8), 16.676 (27), 17.407 (35), 18.697 (34), 19.303 (13), 19.722 (25), 20.641 (11), 21.543 (20), 22.210 (12), 23.229 (16), 23.627 (16), 24.780 (19), 26.533 (6), 27.830 (10), 28.666 (10).

Observed: 9.23 (vs), 10.70 (s), 12.63 (m), 13.75 (m), 15.00 (vs), 15.60 (vw), 16.65 (m), 17.43 (m), 18.70 (m), 19.35 (w), 19.70 (m), 20.65 (vw), 21.55 (vw), 22.25 (vw), 23.23 (w), 23.63 (w), 24.78 (w), 26.55 (vw), 27.75 (vw), 28.68 (vw).

2-(*o*-Hydroxyphenyl)benzothiazoline. A 4.01-g (32.84-mmol) (3.50-mL) sample of salicylaldehyde was dissolved in 80 mL of methanol. To that solution was added 4.11 g (32.84 mmol) (3.51 mL) of 2-aminothiophenol slowly and under continuous stirring. The resulting yellow solution was refluxed with stirring for about 2 h. No color change occurred throughout the reflux period. Then the solution was allowed to cool down to room temperature. Subsequently, the volume of the solution was reduced to ca. 60 mL, and the resulting more concentrated solution was kept at 5 °C for ~12 h. The crystals that formed were isolated by filtration and washed with three 10-mL portions of hexane. Then, they were dried under vacuum. Yield: 5.0 g (~66%).

The FTIR spectrum of the crystalline product shows the N-H vibration at 3256 cm^{-1}. The mass spectrum of the product (electron impact) shows the molecular ion peak at m/e 229.

Bis(tetraethylammonium) Bis[((2-mercaptophenyl)(α-*n*-butylsalicylidene)aminato)(μ-sulfido)ferrate(III)], $[(C_2H_5)_4N]_2[Fe_2S_2(O\text{-}o\text{-}C_6H_4CH(n\text{-}CH_2CH_2CH_2CH_3)NHC_6H_4\text{-}o\text{-}S)_2]$. An amount of $[(C_2H_5)_4N]_2[Fe_2S_2Cl_4]$ (0.39 g, 0.67 mmol) was dissolved in 40 mL of CH_3CN. To a solution of 0.31 g (1.35 mmol) of 2-(*o*-hydroxyphenyl)-benzothiazoline in 10 mL of tetrahydrofuran was added 0.17 g (2.70 mmol, 1.498 mL) of a 2.6 M BuLi solution in hexanes dropwise with a syringe under continuous stirring. The colorless to pale yellow solution that formed was then introduced to the $[(C_2H_5)_4N]_2Fe_2S_2Cl_4$ solution dropwise and under stirring. The resulting reaction mixture was stirred at room temperature for ca. 15 min. The bright red-brown solution was filtered, and to the filtrate was added 90–100 mL of diethyl ether. When this was allowed to stand for ca. 30 h, a red-black microcrystalline material precipitated out of solution. The product was isolated by filtration, washed twice with two 10-mL portions of diethyl ether, and dried under vacuum. The crude product was then recrystallized from a mixture of $CH_3CN/(C_2H_5)_2O$ and afforded 0.40 g of red-black crystals. Yield: ~59%.

Electronic absorption spectrum (CH_3CN solution), λ_{max} (nm); 266 (sh), 290 (sh), 414 (sh), 457.

Calculated powder pattern (2θ values; λ(Cu Kα) = 1.5418 Å; the first 18 lines, with the relative intensities normalized to 100): 5.975 (100.0), 9.386 (30), 10.372 (67), 11.722 (86), 14.089 (11), 15.490 (19), 17.430 (16), 18.442 (41), 19.483 (32), 19.904 (28), 20.355 (35), 21.366 (38), 22.335 (10), 23.665 (9), 25.714 (17), 26.616 (13), 28.384 (12), 29.812 (13).

Observed: 6.00 (vs), 9.40 (m), 10.40 (s), 11.70 (s), 13.95 (vw), 15.50 (w), 17.38 (w), 18.50 (m), 19.52 (m), 19.70 (m), 20.37 (m), 21.30 (m), 22.18 (vw), 23.50 (vw), 25.35 (w), 26.70 (w), 28.28 (vw), 29.40 (w).

Bis(tetraethylammonium) Bis[bis(*p*-methylphenolato)(μ-sulfido)ferrate(III)], $[(C_2H_5)_4N]_2[Fe_2S_2(OC_6H_4\text{-}p\text{-}CH_3)_4]$. An amount of $[(C_2H_5)_4N]_2[Fe_2S_2Cl_4]$ (0.50 g, 0.86 mmol) was dissolved in about 30 mL of CH_3CN. To this solution was added 0.45 g (3.46 mmol) of solid $NaOC_6H_4$-*p*-CH_3 under continuous stirring. The resulting reaction mixture was stirred for ca. 10 min. Immediate color change to bright orange-red occurred upon mixing. The reaction mixture was filtered to remove NaCl, and to the filtrate was added 80–100 mL of diethyl ether. When this was allowed to stand overnight, a deep red microcrystalline material precipitated out of solution. The product was isolated by filtration, washed with two 10-mL portions of diethyl ether, and dried under vacuum. Recrystallization of the crude product from a mixture of $CH_3CN/(C_2H_5)_2O$ afforded 0.58 g of deep red crystals. Yield: 77.6%.

Anal. Calcd for $Fe_2S_2O_4N_2C_{44}H_{68}$ (mol wt 864): C, 61.11; H, 7.87; N, 3.24. Found: C, 60.55; H, 7.45; N, 3.20.

Electronic absorption spectrum (CH_3CN solution), λ_{max} (nm) (ϵ_m); 242 (35 465), 280 (26 100), 414 (12 060), 494 (sh ~7180).

Observed powder pattern (2θ values; λ(Cu Kα) = 1.5418 Å; the first 19 lines): 6.05 (vs), 8.08 (s), 10.65 (s), 12.15 (s), 12.95 (vw), 14.43 (vw), 15.80 (s), 16.80 (vw), 18.83 (s), 19.78 (s), 21.25 (m), 22.88 (s), 24.48 (w), 25.13 (vw), 25.93 (m), 26.90 (vw), 27.75 (w), 28.90 (vw), 29.85 (w).

Bis(tetraphenylphosphonium) Bis[bis(*p*-methylphenolato)(μ-sulfido)ferrate(III)], $[(C_6H_5)_4P]_2[Fe_2S_2(OC_6H_4\text{-}p\text{-}CH_3)_4]$. The tetraphenylphosphonium salt was prepared by a procedure identical with that used to prepare the tetraethylammonium salt. The reactants and the quantities employed in the reaction were as follows: 0.38 g (0.38 mmol) of $[(C_6H_5)_4P]_2[Fe_2S_2Cl_4]$ and 0.20 g (1.53 mmol) of $NaOC_6H_4$-*p*-CH_3 in 35–40 mL of CH_3CN. The product was obtained by addition of diethyl ether to the CH_3CN filtrate of the reaction mixture. Recrystallization of the crude material from a mixture of $CH_3CN/(C_2H_5)_2O$ afforded 0.26 g of bright orange-red microcrystals. Yield: 53.1%.

Anal. Calcd for $Fe_2S_2O_4P_2C_{76}H_{68}$ (mol wt 1282): C, 71.13; H, 5.30. Found: C, 70.08; H, 5.31.

Calculated powder pattern (2θ values; λ(Cu Kα) = 1.5418 Å; the first 18 lines, with the relative intensities normalized to 100): 7.225 (68.8), 8.404 (12.2), 8.971 (12.5), 10.803 (100.0), 11.916 (19.8), 13.257 (43.9), 15.220 (7.1), 16.174 (11.3), 17.508 (6.9), 18.844 (20.4), 19.762 (54.8), 20.903 (33.1), 22.301 (60.6), 24.641 (16.8), 25.268 (8.4), 26.527 (10.9), 27.590 (12.9), 28.164 (14.2).

Observed: 7.23 (s), 8.33 (w), 8.98 (w), 10.80 (vs), 11.90 (w), 13.25 (m), 15.25 (vw), 16.13 (vw), 17.53 (vw), 18.85 (w), 19.80 (s), 20.90 (m), 22.33 (s), 24.63 (w), 25.30 (vw), 26.55 (vw), 27.60 (w), 28.18 (w).

Bis(tetraethylammonium) Bis[bis(*m*-methylphenolato)(μ-sulfido)ferrate(III)], $[(C_2H_5)_4N]_2[Fe_2S_2(OC_6H_4\text{-}m\text{-}CH_3)_4]$. A procedure identical with that employed for the synthesis of the *p*-methylphenolato derivative was followed. The reactants and their quantities used in this reaction were as follows: 0.49 g (0.85 mmol) of $[(C_2H_5)_4N]_2Fe_2S_2Cl_4$ and 0.44 g (3.38 mmol) of $NaOC_6H_4$-*m*-CH_3 in 45 mL of CH_3CN. The deep red to black microcrystalline product obtained was isolated by filtration, washed twice with diethyl ether, and dried under vacuum. Yield: 0.56 g (76.4%).

Anal. Calcd for $Fe_2S_2O_4N_2C_{44}H_{68}$ (mol wt 864): C, 61.11; H, 7.87. Found: C, 61.01; H, 8.11.

Table I. Summary of Crystal Data, Intensity Collection, and Structure Refinement Data for I–IV

	$Fe_2S_2O_4N_2C_{40}H_{56}$ (I)	$Fe_2S_2N_6C_{32}H_{56}$ (II)	$Fe_2S_4O_2N_4C_{50}H_{78}$ (III)	$Fe_2S_2O_4P_2C_{76}H_{68}$ (IV)
mol wt	804	700	1006	1282
a, Å	11.500 (2)	9.689 (3)	14.878 (4)	16.308 (5)
b, Å	13.541 (3)	16.362 (2)	9.585 (3)	16.674 (6)
c, Å	26.612 (5)	11.910 (5)	18.950 (6)	24.456 (9)
α, deg	90.00	90.00	90.00	90.00
β, deg	92.25 (1)	97.74 (3)	95.59 (2)	91.13 (3)
γ, deg	90.00	90.00	90.00	90.00
V, Å^3; Z	4141 (1); 4	1871 (1); 2	2690 (1); 2	6648 (4); 4
d_{calcd}, g/cm^3	1.29	1.24	1.24	1.28
d_{obsd},[a] g/cm^3	1.30	1.32	1.23	1.28
space group	$C2/c$	$P2_1/n$	$P2_1/c$	$P2_1/a$
cryst dimens	b	0.10 × 0.17 × 0.32	0.13 × 0.22 × 0.17	0.25 × 0.20 × 0.05
abs coeff (μ), cm^{-1}	8.07	8.84	6.94	5.59
radiation	Mo ($\lambda_{K\alpha}$ = 0.71069 Å)	Mo ($\lambda_{K\alpha}$ = 0.71069 Å)	Mo ($\lambda_{K\alpha}$ = 0.71069 Å)	Mo ($\lambda_{K\alpha}$ = 0.71069 Å)
data collcd[c]	$h,\pm k,\pm l, 2\theta$ = 45°	$h,k,\pm l$; 2θ = 40°	$h,k,\pm l$; 2θ = 40°	$h,k,\pm l$; 2θ = 40°
scan speed (min–max), deg/min	5.7–29.3	5.0–29.3	2.9–29.3	2.89–29.3
tot. no. of reflcns collcd	6603	2328	2872	6864
R_{merge}[d]	0.024	0.018	0.017	0.034
no. of unique data	2739	1736	2086	3632
no. of data used in refinement $[F_o^2 > 3\sigma(F_o^2)]$	2108	1197	1821	2617[e]
no. of atoms in asymmetric unit	53	37	70	154
no. of variables	310	173	280	385
phasing technique	Patterson	Patterson	direct methods	direct methods
R,[f] %	3.32	6.89	6.46	7.36
R_w,[f] %	3.25	6.96	6.24	6.21

[a] By flotation in CCl_4/pentane mixture. [b] The crystal was accidentally lost before it could be measured. [c] At ambient temperature. [d] $R_{merge} = [\sum_i N_i \sum_{j=1}^{N_i} w(\bar{F}_j - F_j)^2 / \sum (N_i - 1) \sum_{j=1}^{N_i} w F_j^2]^{1/2}$, where N_i is the number of equivalent reflections merged to give the mean $\bar{F}_j$ and F_j is any one of the set. [e] Data used in refinement $F_o^2 > 2.5\sigma(F_o^2)$. [f] $R = [\sum(|F_o| - |F_c|)/\sum|F_o|]$; $R_w = [\sum w(|F_o| - |F_c|)^2 / \sum w|F_o|^2]^{1/2}$.

Observed powder pattern (2θ values; λ(Cu Kα) = 1.5418 Å; the first 16 lines): 6.70 (vs), 10.08 (m), 10.78 (vw), 11.25 (m), 12.28 (w), 13.53 (s), 14.70 (m), 16.08 (vw), 17.48 (vw), 18.681 (s), 19.45 (w), 20.25 (m), 21.20 (m), 23.40 (vw), 24.15 (vw), 24.7 (vw).

X-ray Diffraction Measurements

Collection of Data. Single crystals of $[(C_2H_5)_4N]_2[Fe_2S_2(o,o'\text{-}C_{12}H_8O_2)_2]$ (I), $[(C_2H_5)_4N]_2[Fe_2S_2(C_4H_4N)_4]$ (II), $[(C_2H_5)_4N]_2[Fe_2S_2(O\text{-}o\text{-}C_6H_4CH(n\text{-}Bu)NHC_6H_4\text{-}o\text{-}S)_2]$ (III), and $[(C_6H_5)_4P]_2[Fe_2S_2(OC_6H_4\text{-}p\text{-}CH_3)_4]$ (IV) were obtained by the slow diffusion of diethyl ether into CH_3CN solutions of the respective complexes. The crystals resembled approximately a square prism for I and IV and an oblique quadrangular prism for II and III, respectively. All crystals were mounted in thin-walled capillary tubes, which were sealed as a precaution against air and moisture sensitivity. The X-ray crystallographic data were obtained on a Nicolet P3/F four-circle computer-controlled diffractometer. A detailed description of the instrument and the data acquisition procedures have been given previously.[20] Intensity data were collected on one-fourth of the reciprocal lattice sphere for II, III, and IV and half of the reciprocal lattice sphere for I. The data were obtained by using graphite-monochromatized Mo Kα radiation.

For each of the four structures, the unit cell was determined from 12 well-centered reflections whose x and y coordinates were obtained from random orientation photographs. Accurate cell parameters were obtained from a least-squares fit of the angular settings (2θ, ω, ϕ, χ) of 25 machine-centered reflections with 2θ values between 20 and 40°.

Details concerning crystal characteristics and X-ray diffraction methodology are shown in Table I.

Reduction of Data. The raw data were reduced to net intensities, estimated standard deviations were calculated on the basis of counting statistics, Lorentz–polarization corrections were applied, and equivalent reflections were averaged. The estimated standard deviation of the structure factor was taken as the larger of that derived from counting statistics and that derived from the scatter of multiple measurements.

The least squares program used minimizes $\sum w(\Delta|F|)^2$. The weighting function used throughout the refinement of the structure gives zero weight to those reflections with $F^2 \leq 3\sigma(F^2)$ and $w = 1/\sigma^2(F)$ to all others,[21a] where $\sigma^2(F) = \sigma_1^2(F) + \text{abs}(g)\,F^2$ (g = 0.0002). No corrections for secondary extinction were applied to data sets I through IV. The atomic scattering factors of the neutral atoms were used[21b] and all the scattering factors except those for hydrogen[21c] were corrected by adding real and imaginary terms to account for the effects of anomalous dispersion.[21d]

Due to the small μ values (Table I) and the size of the crystals, no absorption corrections were applied. The refinement calculations were carried out on The University of Michigan Amdahl 800 computer using the locally adapted SHELX76 crystallographic program package.

Determination of Structures. (i) $[(C_2H_5)_4N]_2[Fe_2S_2(o,o'\text{-}C_{12}H_8O_2)_2]$ (I). The systematic absences hkl ($h + k \neq 2n$), $h0l$ ($l \neq 2n$; $h \neq 2n$), and $0k0$ ($k \neq 2n$) for the monoclinic cell limited the choice of space groups to $C2/c$ and Cc. Statistical analysis of intensities led to the former, centrosymmetric space group, and subsequent successful solution and refinement of the structure confirmed this choice.

The $[Fe_2S_2(o,o'\text{-}C_{12}H_8O_2)_2]^{2-}$ anion is required by symmetry to reside on a crystallographic inversion center. The Fe–S unique fragment of the $[Fe_2S_2]^{2+}$ core was initially located from the Patterson map, and the rest of the non-hydrogen atoms were found with successive electron density difference Fourier maps following least-squares refinement[22] of the input atomic coordinates. The refinement of all the atoms in the asymmetric unit with isotropic temperature factors gave a conventional R value of 0.128. The refinement process then continued (full-matrix least-squares techniques), assigning anisotropic temperature factors to all non-hydrogen atoms in the asymmetric unit. The hydrogen atoms in the asymmetric unit were easily located from an electron density

(20) Kanatzidis, M. G.; Coucouvanis, D. *Inorg. Chem.* **1984**, *23*, 403.

(21) (a) Grant, D. F.; Killean, R. C. G.; Lawrence, J. L. *Acta Crystallogr., Sect. B: Struct. Crystallogr. Cryst. Chem.* **1969**, *B25*, 374. (b) Doyle, P. A.; Turner, P. S. *Acta Crystallogr., Cryst. Phys., Diffr., Theor. Gen. Crystallogr.* **1968**, *A24*, 390. (c) Stewart, R. F.; Davidson, E. R.; Simpson, W. T. *J. Chem. Phys.* **1965**, *42*, 3175. (d) Cromer, D. T.; Liberman, D. *J. Chem. Phys.* **1970**, *53*, 1891.

(22) SHELXTL package of crystallographic programs, Nicolet XRD Corp., Fremont, CA.

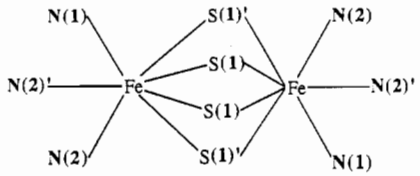

Figure 1. Mode of disorder in $[(C_2H_5)_4N]_2Fe_2S_2(C_4H_4N)_4$.

map. The final R value was 0.033, and the weighted R_w was 0.032. During the last cycle of refinement, all parameter shifts were less than 10% of their estimated standard deviation.

(ii) $[(C_2H_5)_4N]_2[Fe_2S_2(C_4H_4N)_4]$ (II). A sharpened three-dimensional Patterson synthesis map was used to solve the structure, followed by Fourier electron density calculations using the SHELXTL and SHELX76 packages of crystallographic programs.

The $[Fe_2S_2(C_4H_4N)_4]^{2-}$ anion is required by symmetry to reside on a crystallographic inversion center. The Fe–S unique fragment of the $[Fe_2S_2]^{2+}$ core was initially located from the Patterson map. The rest of the non-hydrogen atoms were found in successive Fourier electron density maps. The tetraethylammonium ($(C_2H_5)_4N^+$) cation located in the asymmetric unit was found to be positionally disordered with approximate 50% occupancy. Positional disorder was also observed for the bridging sulfur atom and one of the terminal pyrrolate ligands. The disordered pyrrolate ligand occupies two positions with equal weight around one of the tetrahedral sites of the iron atom. The mode of disorder is shown in Figure 1. The refinement of all the atoms in the asymmetric unit with isotropic temperature factors resulted in an R value of 0.107. The refinement process continued (full-matrix least-squares techniques), assigning anisotropic temperature factors to all non-hydrogen atoms in the asymmetric unit that were not disordered. An attempt was made to refine the disordered pyrrole rings with anisotropic temperature factors. It resulted in the appearance of nonpositive definite temperature factors for one of the carbon atoms. This undoubtedly is due to the marginal quality of the data that was measured on the best obtainable but still poor quality crystal. At this stage, the hydrogen atom positions were calculated only for those atoms that were nondisordered and were included in the structure factor calculation but were not refined. The final R values was 0.069, and the weighted R_w was 0.070. During the last cycle of refinement, all parameter shifts were less than 10% of their esd.

(iii) $[(C_2H_5)_4N]_2[Fe_2S_2(O\text{-}o\text{-}C_6H_4CH(n\text{-}CH_2CH_2CH_2CH_3)NHC_6H_4\text{-}o\text{-}S)_2]$ (III). The $[Fe_2S_2(O\text{-}o\text{-}C_6H_4CH(n\text{-}CH_2CH_2CH_2CH_3)NHC_6H_4\text{-}o\text{-}S)_2]^{2-}$ anion is required by symmetry to reside on a crystallographic inversion center. The Fe–S unique fragment of the $[Fe_2S_2]^{2+}$ core along with the oxygen and sulfur terminal atoms of the chelate ligand were initially located by direct methods.[22] The rest of the non-hydrogen atoms were located with successive electron density difference Fourier maps following least-squares refinement of the input atomic coordinates. The refinement of all the atoms in the asymmetric unit with isotropic temperature factors resulted in an R value of 0.133. The refinement process continued (full-matrix least-squares techniques), assigning anisotropic temperature factors to all non-hydrogen atoms in the asymmetric unit and gave an R value of 0.085. At this stage, the positions of the hydrogen atoms were calculated. The position of the hydrogen atom corresponding to the nitrogen atom of the chelate ligand was not calculated and therefore not included in the structure factor calculation. In the final refinement cycle, the hydrogen atoms were included in the structure factor calculation, but were not refined. The final R value was 0.065, and R_w was 0.062. During the last cycle of refinement, all parameter shifts were less than 10% of their esd.

(iv) $[(C_6H_5)_4P]_2[Fe_2S_2(OC_6H_4\text{-}p\text{-}CH_3)_4]$ (IV). The structure was solved by direct methods using the SOLV routine of the SHELXTL package of crystallographic programs,[22] followed by Fourier electron density calculations performed with SHELXTL as well as SHELX76.

Two Fe–S unique fragments belonging to two $[Fe_2S_2]^{2+}$ cores were initially located from direct methods. The rest of the non-hydrogen atoms were located with successive electron density difference Fourier maps following least-squares refinement of the input atomic coordinates. The two $[Fe_2S_2(OC_6H_4\text{-}p\text{-}CH_3)_4]^{2-}$ anions in the unit cell are located on centers of symmetry at $^1/_2$, $^1/_2$, $^1/_2$ and 0, $^1/_2$, 0. The non-carbon atoms in the two independent half-anions and the P atoms in the two independent Ph_4P^+ cations appear to be related by an approximate, noncrystallographic screw axis such that $x_i = {}^1/_2 - x_j$, $y_i = -y_j$, and $z_i = {}^1/_2 + z_j$. A close examination shows that the positions of the C atoms do not adhere to this relationship, and the phenyl rings in the two anions adopt entirely different relative orientations. This indicates that the observed relationship in the positional coordinates of the heavier atoms does not reflect an erroneous choice of unit cell but rather an accidental, albeit intriguing, occurrence. The refinement of all the atoms in the asymmetric unit with isotropic temperature factors gave a conventional R value of 0.133. The refinement process continued (full-matrix least-squares techniques), assigning anisotropic temperature factors to the iron, sulfur, and oxygen atoms of the two unique Fe–S fragments in the asymmetric unit. At this stage, the hydrogen atom positions were calculated. In the final stage of refinement, they were included in the structure factor calculation but were not refined. The final R value was 0.074, and the weighted R_w was 0.062. During the last cycle of refinement, all parameter shifts were less than 10% of their estimated standard deviation (esd).

Table II. Positional[a] and Equivalent Isotropic Thermal Parameters[b] for the Non-Hydrogen Atoms in $[Et_4N]_2Fe_2S_2(o,o'\text{-}C_{12}H_8O_2)_2$

atom	x	y	z	U_{eq}, Å^2
Fe	0.6942	0.2162	0.0402	0.044
S(1)	0.8813 (1)	0.1999 (1)	0.0244	0.055
O(1)	0.6638 (2)	0.2784 (2)	0.1021 (1)	0.046
O(2)	0.6255 (2)	0.0936 (2)	0.0558 (1)	0.043
C(1)	0.5352 (3)	0.0810 (2)	0.0855 (1)	0.041
C(2)	0.4345 (3)	0.0361 (3)	0.0651 (1)	0.054
C(3)	0.3418 (3)	0.0134 (3)	0.0949 (2)	0.068
C(4)	0.3483 (4)	0.0353 (3)	0.1451 (2)	0.069
C(5)	0.4459 (3)	0.0797 (3)	0.1658 (1)	0.054
C(6)	0.5415 (3)	0.1043 (2)	0.1370 (1)	0.039
C(7)	0.6462 (3)	0.1484 (2)	0.1627 (1)	0.042
C(8)	0.6897 (4)	0.1075 (3)	0.2079 (1)	0.057
C(9)	0.7871 (4)	0.1444 (4)	0.2328 (2)	0.077
C(10)	0.8433 (4)	0.2235 (4)	0.2135 (2)	0.084
C(11)	0.8030 (4)	0.2666 (3)	0.1696 (2)	0.065
C(12)	0.7040 (3)	0.2316 (3)	0.1437 (1)	0.043
N	0.3383 (2)	0.3845 (2)	0.1137 (1)	0.050
C(13)	0.3656 (6)	0.3617 (5)	0.2081 (3)	0.108
C(14)	0.3902 (4)	0.3249 (3)	0.1568 (2)	0.071
C(15)	0.1460 (5)	0.2913 (5)	0.1165 (3)	0.096
C(16)	0.2070 (3)	0.3900 (3)	0.1158 (2)	0.059
C(17)	0.3813 (4)	0.4905 (3)	0.1163 (2)	0.060
C(18)	0.5109 (4)	0.5028 (4)	0.1147 (3)	0.097
C(19)	0.3741 (4)	0.3346 (4)	0.0660 (2)	0.076
C(20)	0.3292 (6)	0.3831 (5)	0.0190 (2)	0.108

[a] Calculated standard deviations are indicated in parentheses. [b] The form of U_{eq} is $U_{eq} = {}^1/_3 \sum_i \sum_j U_{ij} a_i^* a_j^* \mathbf{a}_i \cdot \mathbf{a}_j$.

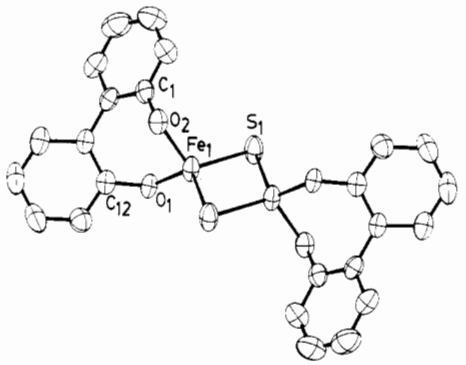

Figure 2. Structure and labeling of the $[Fe_2S_2(o,o'\text{-}C_{12}H_8O_2)_2]^{2-}$ anion as drawn by ORTEP.

Crystallographic Results. The final atomic positional and thermal parameters of $[(C_2H_5)_4N]_2[Fe_2S_2(o,o'\text{-}C_{12}H_8O_2)_2]$,

Table III. Positional[a] and Equivalent Isotropic Thermal Parameters[b] for the Non-Hydrogen Atoms in $[Et_4N]_2Fe_2S_2(C_4H_4N)_4$

atom	x	y	z	U_{eq}, Å^2
Fe	0.0253 (2)	1.0497 (1)	0.0896 (1)	0.057
S(1)′	0.0802 (8)	0.9134 (5)	0.0675 (6)	0.047
S(1)	−0.1135 (8)	1.0653 (5)	−0.0789 (6)	0.053
N(1)	−0.0863 (11)	1.0649 (7)	0.2138 (8)	0.076
C(1)	−0.0424 (16)	1.0456 (10)	0.3265 (12)	0.096
C(2)	−0.1375 (19)	1.0709 (9)	0.3930 (11)	0.089
C(3)	−0.2439 (16)	1.1043 (9)	0.3240 (14)	0.088
C(4)	−0.2139 (14)	1.1004 (8)	0.2136 (11)	0.073
N(2)	0.1815 (22)	1.1385 (14)	0.0966 (19)	0.043
C(5)	0.1663 (25)	1.2192 (14)	0.0554 (18)	0.050
C(6)	0.2712 (34)	1.2650 (17)	0.1085 (25)	0.075
C(7)	0.3666 (30)	1.1955 (19)	0.1775 (26)	0.067
C(8)	0.2938 (32)	1.1328 (17)	0.1648 (25)	0.072
N(2)′	0.1854 (25)	1.1075 (14)	0.1489 (21)	0.064
C(5)′	0.2609 (30)	1.1123 (15)	0.2539 (24)	0.072
C(6)′	0.3730 (31)	1.1726 (17)	0.2520 (27)	0.095
C(7)′	0.3623 (63)	1.2259 (33)	0.1558 (46)	0.086
C(8)′	0.2399 (37)	1.1709 (20)	0.0792 (25)	0.077
N	0.4110 (18)	0.1196 (9)	0.8013 (13)	0.032
C(C1)	0.2623 (29)	0.0937 (16)	0.7883 (22)	0.064
C(C2)	0.1762 (16)	0.1684 (9)	0.7397 (12)	0.098
C(C3)	0.4344 (22)	0.1903 (12)	0.8863 (17)	0.048
C(C4)	0.5760 (14)	0.2179 (7)	0.8997 (11)	0.076
C(C5)	0.4211 (32)	0.0830 (17)	0.5936 (26)	0.094
C(C6)	0.5058 (25)	0.0495 (15)	0.8348 (19)	0.070
C(C7)	0.4857 (30)	0.0154 (16)	0.9574 (19)	0.080
N′	0.4484 (11)	0.1535 (6)	0.6996 (8)	0.076
C(C1)′	0.5115 (24)	0.2312 (12)	0.7729 (18)	0.054
C(C2)′	0.3202 (30)	0.1216 (14)	0.7493 (21)	0.053
C(C3)′	0.4018 (24)	0.1853 (13)	0.5831 (18)	0.054
C(C4)′	0.3480 (25)	0.1216 (13)	0.5095 (19)	0.059
C(C5)′	0.5480 (25)	0.0857 (14)	0.7104 (18)	0.058
C(C6)′	0.6737 (29)	0.1028 (16)	0.6549 (22)	0.082

[a] Calculated standard deviations are indicated in parentheses. [b] The form of U_{eq} is $U_{eq} = {}^1/_3 \sum_i \sum_j U_{ij} a_i^* a_j^* \mathbf{a}_i \cdot \mathbf{a}_j$.

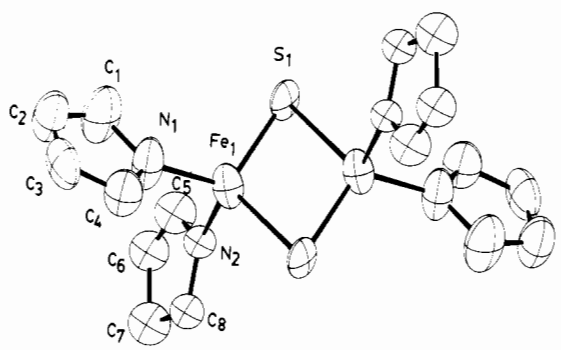

Figure 3. Structure and labeling of the $[Fe_2S_2(C_4H_4N)_4]^{2-}$ anion. Due to a positional disorder in the $C_5C_6C_7C_8N_2$ ligand, only one of the components is shown in the figure.

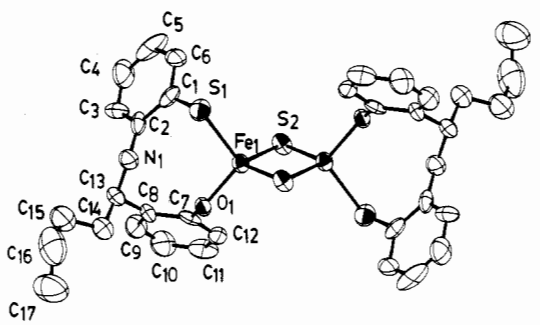

Figure 4. Structure and labeling of the $[Fe_2S_2(O\text{-}o\text{-}C_6H_4CH(n\text{-}Bu)NHC_6H_4\text{-}o\text{-}S)_2]^{2-}$ anion. Thermal ellipsoids as drawn by ORTEP represent the 50% probability surfaces.

$[(C_2H_5)_4N]_2[Fe_2S_2(C_4H_4N)_4]$, $[(C_2H_5)_4N]_2[Fe_2S_2(O\text{-}o\text{-}C_6H_4CH(n\text{-}Bu)NHC_6H_4\text{-}o\text{-}S)_2]$, and $[(C_6H_5)_4P]_2[Fe_2S_2(OC_6H_4\text{-}p\text{-}CH_3)_4]$, with standard deviations derived from the inverse matrices of the least squares refinements, are compiled in Tables II–V, respectively.

Intramolecular distances and angles for the anions in all structures are given in Tables VI–IX. The atom-labeling schemes are shown in Figures 2–5.

Table IV. Positional[a] and Equivalent Isotropic Thermal Parameters[b] for the Non-Hydrogen Atoms in $[Et_4N]_2Fe_2S_2(O\text{-}o\text{-}C_6H_4CH(n\text{-}Bu)NHC_6H_4\text{-}o\text{-}S)_2$

atom	x	y	z	U_{eq}, Å^2
Fe (1)	0.4291 (2)	0.5202 (3)	0.4506 (1)	0.0340
S(1)	0.4415 (3)	0.5179 (6)	0.3301 (2)	0.0513
S(2)	0.5270 (3)	0.6760 (5)	0.4968 (3)	0.0410
O(1)	0.3054 (7)	0.5644 (12)	0.4616 (6)	0.0373
C(1)	0.3645 (14)	0.3805 (21)	0.3004 (8)	0.0456
C(2)	0.2698 (12)	0.3968 (25)	0.3002 (9)	0.0434
C(3)	0.2154 (14)	0.2821 (25)	0.2778 (11)	0.0567
C(4)	0.2499 (16)	0.1640 (31)	0.2529 (12)	0.0777
C(5)	0.3392 (23)	0.1485 (21)	0.2499 (11)	0.0836
C(6)	0.3985 (14)	0.2532 (28)	0.2740 (10)	0.0615
C(7)	0.2366 (11)	0.4788 (19)	0.4775 (10)	0.0381
C(8)	0.1615 (12)	0.4562 (20)	0.4274 (10)	0.0418
C(9)	0.0929 (13)	0.3748 (24)	0.4464 (12)	0.0571
C(10)	0.0943 (14)	0.3143 (26)	0.5116 (14)	0.0711
C(11)	0.1654 (15)	0.3374 (22)	0.5605 (11)	0.0619
C(12)	0.2379 (13)	0.4167 (20)	0.5438 (10)	0.0431
C(13)	0.1533 (11)	0.5284 (21)	0.3556 (10)	0.0478
C(14)	0.1251 (13)	0.6781 (22)	0.3605 (11)	0.0588
C(15)	0.0886 (15)	0.7395 (29)	0.2913 (13)	0.0832
C(16)	0.0736 (20)	0.8955 (39)	0.2931 (17)	0.1197
C(17)	0.0205 (22)	0.9540 (32)	0.3419 (16)	0.1306
N(1)	0.2344 (10)	0.5247 (16)	0.3186 (7)	0.0447
N(2)	0.3053 (10)	0.5812 (15)	0.0770 (8)	0.0448
C(18)	0.3581 (13)	0.4632 (20)	0.1168 (10)	0.0550
C(19)	0.4599 (15)	0.4749 (21)	0.1184 (10)	0.0655
C(20)	0.3376 (13)	0.7227 (21)	0.1051 (10)	0.0554
C(21)	0.3223 (15)	0.7509 (22)	0.1818 (11)	0.0698
C(22)	0.2068 (12)	0.5578 (23)	0.0883 (11)	0.0633
C(23)	0.1420 (14)	0.6670 (27)	0.0545 (13)	0.0924
C(24)	0.3186 (12)	0.5816 (21)	−0.0015 (10)	0.0492
C(25)	0.2857 (15)	0.4507 (22)	−0.0408 (11)	0.0700

[a] Calculated standard deviations are indicated in parentheses. [b] The form of U_{eq} is $U_{eq} = {}^1/_3 \sum_i \sum_j U_{ij} a_i^* a_j^* \mathbf{a}_i \cdot \mathbf{a}_j$.

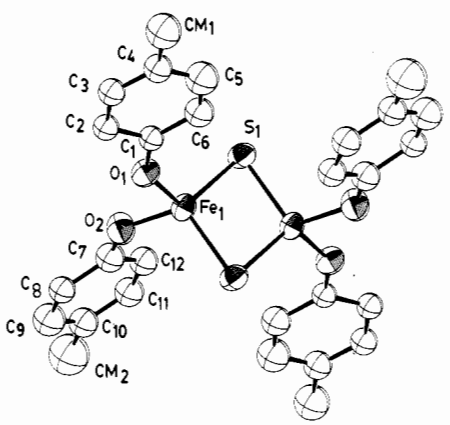

Figure 5. Structure and labeling of the $[Fe_2S_2(OC_6H_4\text{-}p\text{-}CH_3)_4]^{2-}$ anion (A). Thermal ellipsoids as drawn by ORTEP represent the 50% probability surfaces.

Results and Discussion

Synthesis. The syntheses of the aryloxide $[Fe_2S_2L_4]^{2-}$ dimers (L_2 = $o,o'\text{-}C_{12}H_8O_2^{2-}$ (I), L_2 = $(O\text{-}o\text{-}C_6H_4CH(n\text{-}Bu)NHC_6H_4\text{-}o\text{-}S)^{2-}$ (III), L = $^-OC_6H_4\text{-}p\text{-}CH_3$ (IV), and $^-O\text{-}C_6H_4\text{-}m\text{-}CH_3$ (V)) and of the analogous pyrrolate complex $[Fe_2S_2(C_4H_4N)_4]^{2-}$ (II) are accomplished readily by metathetical reactions. These stoichiometric reactions occur in CH_3CN solution under *strictly* anaerobic and moisture-free conditions between the $[Fe_2S_2Cl_4]^{2-}$ anion and the alkali-metal salts of the ligands. The new dimeric complexes are obtained in pure crystalline form as tetraalkylammonium or tetraphenyl phosphonium salts.

Table V. Positional[a] and Equivalent Isotropic Thermal Parameters[b] for the Non-Hydrogen Atoms in $(Ph_4P)_2[Fe_2S_2(OC_6H_4\text{-}p\text{-}CH_3)_4]$

atom	x	y	z	U_{eq}, Å^2	atom	x	y	z	U_{eq}, Å^2
Fe(1)	0.4529 (1)	0.5684 (1)	0.4922 (1)	0.0410	C(31)	0.4716 (10)	0.5711 (10)	0.1117 (6)	0.0466
Fe(2)	0.0488 (2)	0.5663 (2)	−0.0009 (1)	0.0565	C(32)	0.4058 (11)	0.6148 (12)	0.1323 (7)	0.0742
S(1)	0.4286 (2)	0.4442 (3)	0.4622 (2)	0.0484	C(33)	0.4031 (12)	0.7000 (13)	0.1244 (8)	0.0943
S(2)	−0.0699 (3)	0.5514 (3)	0.0409 (2)	0.0651	C(34)	0.4627 (13)	0.7351 (12)	0.0956 (8)	0.0868
O(1)	0.4464 (6)	0.6446 (6)	0.4356 (4)	0.0610	C(35)	0.5263 (10)	0.6956 (11)	0.0741 (7)	0.0630
O(2)	0.3685 (6)	0.6167 (6)	0.5313 (4)	0.0528	C(36)	0.5336 (10)	0.6123 (11)	0.0820 (7)	0.0609
O(3)	0.0513 (7)	0.6465 (7)	−0.0534 (5)	0.0857	C(37)	0.5770 (9)	0.4330 (10)	0.1026 (7)	0.0518
O(4)	0.1329 (6)	0.6067 (7)	0.0445 (5)	0.0780	C(38)	0.6399 (11)	0.4486 (12)	0.1395 (7)	0.0843
C(1)	0.4834 (11)	0.6548 (10)	0.3886 (8)	0.0552	C(39)	0.7210 (11)	0.4310 (12)	0.1231 (8)	0.0861
C(2)	0.4385 (9)	0.6892 (9)	0.3432 (7)	0.0457	C(40)	0.7343 (10)	0.3977 (10)	0.0748 (8)	0.0651
C(3)	0.4770 (11)	0.7026 (10)	0.2934 (7)	0.0688	C(41)	0.6741 (11)	0.3787 (10)	0.0379 (7)	0.0588
C(4)	0.5541 (10)	0.6770 (10)	0.2853 (7)	0.0557	C(42)	0.5923 (10)	0.3993 (9)	0.0522 (7)	0.0526
C(5)	0.5987 (9)	0.6445 (10)	0.3277 (7)	0.0555	C(43)	0.4572 (9)	0.4425 (11)	0.1897 (6)	0.0509
C(6)	0.5650 (10)	0.6311 (9)	0.3779 (7)	0.0524	C(44)	0.4738 (10)	0.4947 (10)	0.2318 (8)	0.0649
C(M1)	0.5962 (12)	0.6924 (12)	0.2314 (8)	0.1072	C(45)	0.4596 (10)	0.4769 (11)	0.2871 (8)	0.0685
C(7)	0.3338 (9)	0.6179 (9)	0.5800 (7)	0.0399	C(46)	0.4293 (11)	0.4039 (13)	0.2987 (8)	0.0822
C(8)	0.2648 (9)	0.6675 (9)	0.5864 (6)	0.0439	C(47)	0.4131 (15)	0.3520 (15)	0.2596 (12)	0.1498
C(9)	0.2264 (9)	0.6678 (9)	0.6373 (7)	0.0479	C(48)	0.4275 (13)	0.3692 (14)	0.2040 (9)	0.1137
C(10)	0.2507 (10)	0.6235 (10)	0.6801 (7)	0.0523	P(2)	0.9734 (3)	0.5345 (3)	0.3779 (2)	0.0406
C(11)	0.3188 (10)	0.5763 (11)	0.6741 (7)	0.0721	C(49)	0.8975 (8)	0.5799 (9)	0.4206 (6)	0.0377
C(12)	0.3611 (9)	0.5735 (10)	0.6251 (7)	0.0563	C(50)	0.8211 (9)	0.5411 (8)	0.4227 (6)	0.0365
C(M2)	0.2058 (10)	0.6228 (11)	0.7347 (8)	0.0815	C(51)	0.7596 (9)	0.5769 (10)	0.4538 (6)	0.0477
C(13)	0.0016 (11)	0.6603 (10)	−0.0964 (8)	0.0579	C(52)	0.7742 (9)	0.6491 (10)	0.4787 (6)	0.0472
C(14)	0.0275 (11)	0.6494 (11)	−0.1489 (9)	0.0772	C(53)	0.8484 (9)	0.6888 (9)	0.4750 (6)	0.0456
C(15)	−0.0217 (13)	0.6679 (12)	−0.1947 (8)	0.0930	C(54)	0.9092 (9)	0.6542 (9)	0.4447 (6)	0.0380
C(16)	−0.1006 (14)	0.6969 (13)	−0.1864 (10)	0.1028	C(55)	1.0746 (8)	0.5723 (10)	0.3944 (6)	0.0366
C(17)	−0.1270 (11)	0.7074 (11)	−0.1336 (9)	0.0780	C(56)	1.1314 (10)	0.5222 (9)	0.4217 (7)	0.0530
C(18)	−0.0766 (11)	0.6894 (10)	−0.0897 (7)	0.0690	C(57)	1.2084 (10)	0.5524 (11)	0.4332 (6)	0.0603
C(M3)	−0.1559 (14)	0.7126 (15)	−0.2343 (10)	0.1588	C(58)	1.2286 (10)	0.6305 (11)	0.4193 (7)	0.0565
C(19)	0.1577 (10)	0.5907 (12)	0.0958 (8)	0.0606	C(59)	1.1728 (11)	0.6785 (10)	0.3917 (7)	0.0657
C(20)	0.1865 (11)	0.6576 (12)	0.1268 (9)	0.0906	C(60)	1.0954 (10)	0.6492 (11)	0.3780 (7)	0.0551
C(21)	0.2136 (11)	0.6423 (13)	0.1813 (9)	0.0904	C(61)	0.9745 (9)	0.4294 (9)	0.3912 (6)	0.0409
C(22)	0.2120 (11)	0.5711 (14)	0.2029 (8)	0.0859	C(62)	0.9494 (9)	0.3950 (10)	0.4390 (6)	0.0443
C(23)	0.1880 (11)	0.5059 (12)	0.1724 (9)	0.0860	C(63)	0.9556 (9)	0.3149 (11)	0.4481 (7)	0.0535
C(24)	0.1575 (10)	0.5186 (11)	0.1192 (8)	0.0635	C(64)	0.9931 (10)	0.2651 (11)	0.4119 (8)	0.0655
C(M4)	0.2446 (14)	0.5503 (14)	0.2623 (10)	0.1580	C(65)	1.0200 (11)	0.2974 (12)	0.3644 (8)	0.0815
P(1)	0.4755 (3)	0.4660 (3)	0.1202 (2)	0.0467	C(66)	1.0083 (10)	0.3799 (11)	0.3508 (7)	0.0627
C(25)	0.4006 (9)	0.4203 (10)	0.0772 (6)	0.0461	C(67)	0.9487 (9)	0.5560 (9)	0.3094 (6)	0.0453
C(26)	0.3370 (9)	0.4648 (9)	0.0536 (6)	0.0497	C(68)	1.0046 (9)	0.5493 (10)	0.2673 (7)	0.0576
C(27)	0.2776 (10)	0.4265 (11)	0.0214 (6)	0.0618	C(69)	0.9837 (10)	0.5633 (11)	0.2117 (7)	0.0711
C(28)	0.2785 (10)	0.3453 (11)	0.0119 (7)	0.0575	C(70)	0.9062 (11)	0.5865 (10)	0.1987 (7)	0.0647
C(29)	0.3406 (11)	0.3001 (10)	0.0358 (7)	0.0660	C(71)	0.8480 (10)	0.5973 (10)	0.2381 (8)	0.0663
C(30)	0.4006 (10)	0.3369 (10)	0.0683 (7)	0.0560	C(72)	0.8696 (9)	0.5826 (10)	0.2931 (7)	0.0555

[a] Calculated standard deviations are indicated in parentheses. [b] The form of U_{eq} is $U_{eq} = {}^1/_3\sum_i\sum_j U_{ij}a_i^*a_j^*\mathbf{a}_i\cdot\mathbf{a}_j$.

Scheme I

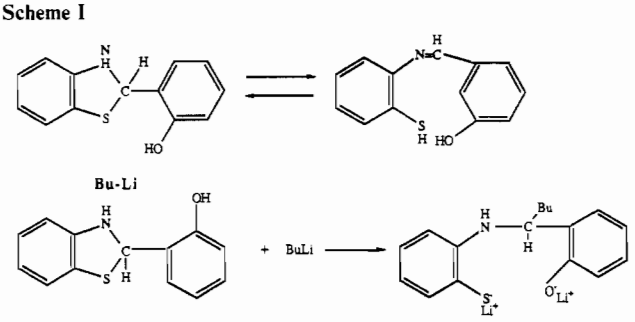

The $[L_2FeS_2FeL_2]^{2-}$ clusters I–IV exhibit exceedingly high hydrolytic and solvolytic instability not unlike that encountered previously for the $[Fe(OC_6H_5)_4]^-$,[23] $[Fe_6S_6(OAr)_6]^{3-}$,[24] and $[Fe_4S_4(OAr)_{4-x}L_x]^{2-}$ (x = 0, 2;[25] L = Cl^-, $^-SC_6H_5$)[26] complexes. The chelating ligand in III was obtained by the reaction of *n*-BuLi with 2-(*o*-hydroxyphenyl)benzothiazoline. The latter is obtained in the reaction between salicylaldehyde and *o*-aminothiophenol and has been used previously[27] as a source for the tautomeric Schiff base [((2-mercaptophenyl)imino)methyl]-2-hydroxybenzene (Scheme I).

Addition of *n*-BuLi into a THF solution of 2-(*o*-hydroxyphenyl)benzothiazoline apparently results in an attack of the butyl group on the electrophilic carbon atom of the benzothiazolinic ring with concomitant opening of the latter and subsequent deprotonation and formation of the dilithium salt of the C-alkylated form of the ligand. The latter is used in the metathetical reaction that produces III. The reactivity I–IV toward electrophiles such as benzoyl chloride (C_6H_5COCl) is similar to that of the thiophenolate dimers. Rapid reactions occur upon the addition of C_6H_5COCl to CH_3CN solutions of the complexes, leading to the formation of $[Fe_2S_2Cl_4]^{2-}$. The aryloxide and pyrrolate dimers also react instantly and quantitatively with either aliphatic or aromatic thiols to afford the analogous thiolate dimers.

Crystallographic Studies. $[(C_2H_5)_4N]_2[Fe_2S_2(o,o'\text{-}C_{12}H_8O_2)_2]$ (I). The compound crystallizes in space group $C2/c$ of the monoclinic system with four molecules per unit cell. The crystal structure consists of discrete cations and anions. The tetraethylammonium cations have their expected unexceptional geometry with a mean C_i–N–C_j angle of 109.5 (9)° and a mean

(23) Koch, S. A.; Millar, M. *J. Am. Chem. Soc.* **1982**, *104*, 5255.
(24) Kanatzidis, M. G.; Salifoglou, A.; Coucouvanis, D. *Inorg. Chem.* **1986**, *25*, 2460.
(25) Cleland, W. E.; Holtman, D. A.; Sabat, M.; Ibers, J. A.; Defotis, G. C.; Averill, B. A. *J. Am. Chem. Soc.* **1983**, *105*, 6021.
(26) Kanatzidis, M. G.; Baenziger, N. C.; Coucouvanis, D.; Simopoulos, A.; Kostikas, A. *J. Am. Chem. Soc.* **1984**, *106*, 4500.
(27) (a) Charles, R. G.; Freiser, H. *J. Org. Chem.* **1953**, *18*, 422. (b) Lindoy, L. F.; Livingstone, S. E. *Inorg. Chim. Acta* **1967**, *1*, 365. (c) Alyea, E. C.; Malek, A. *Can. J. Chem.* **1975**, *53*, 939. (d) Lindoy, L. F.; Busch, D. H. *Inorg. Chem.* **1974**, *13*, 2494. (e) Alyea, E. C.; Malek, A.; Merrell, P. H. *J. Coord. Chem.* **1974**, *4*, 55. (f) Cimerman, Z.; Stefanac, Z. *Polyhedron* **1985**, *4*, 1755. (g) Casellato, V.; Vigato, P. A.; Vidali, M. *Coord. Chem. Rev.* **1977**, *23*, 31.

Table VI. Selected Distances (Å) and Angles (deg) in the Anion[a] of the $(C_2H_5)_4N^+$ Salt of $Fe_2S_2(o,o'\text{-}C_{12}H_8O_2)_2^{2-}$

	Distances		
Fe–S(1)	2.220 (1)	Fe–O(1)	1.895 (2)
Fe–S(1)	2.209 (1)	Fe–O(2)	1.892 (2)
mean	2.215 (6)	mean	1.894 (2)
Fe···Fe	3.699 (1)	S(1)···S(1)	3.512 (2)
	Angles		
Fe–S(1)–Fe	75.1 (1)	S(1)–Fe–S(1)	104.9 (1)
S(1)–Fe–O(1)	111.1 (1)		
S(1)–Fe–O(2)	111.8 (1)		
S(1)–Fe–O(1)	115.5 (1)		
S(1)–Fe–O(2)	117.8 (1)		
O(1)–Fe–O(2)	96.1 (1)	Fe–O(2)–C(1)	125.5 (2)
		Fe–O(1)–C(12)	116.0 (2)

[a] For the cation in $[(C_2H_5)_4N]_2Fe_2S_2(o,o'\text{-}C_{12}H_8O_2)_2$, the N-C bonds are within the range 1.506 (5)–1.519 (5) Å with a mean value of 1.513 (5) Å. The C–C bonds are within the range 1.493 (8)–1.510 (7) Å with a mean value of 1.498 (8) Å. The six C_i–N–C_j angles are found between 106.0 (3) and 111.4 (3)° with a mean value of 109.5 (9)°. The N–C_i–C_j angles are found between 114.5 (4) and 115.6 (4)° with a mean value of 115.0 (4)°. In this table and Tables VII and VIII, the standard deviations from the mean have been obtained as follows: $\sigma = [\sum_{i=1}^{N} (x_i - \bar{x})^2/N(N-1)]^{1/2}$, where x_i is the value of an individual bond or angle and $\bar{x}$ is the mean value for the N equivalent bond lengths or angles.

Table VII. Selected Distances (Å) and Angles (deg) in the Anion[a] of the $(C_2H_5)_4N^+$ Salt of $Fe_2S_2(C_4H_4N)_4^{2-}$

	Distances		
Fe–S(1)	2.275 (8)	Fe–S(1)′	2.316 (8)
Fe–S(1)	2.078 (8)	Fe–S(1)′	2.096 (8)
Fe···Fe	2.677 (3)	Fe···Fe	2.677 (3)
S(1)···S(1)	3.439 (15)	S(1)′···S(1)′	3.515 (15)
Fe–N(1)	1.962 (10)	Fe–N(1)	1.962 (10)
Fe–N(2)	2.092 (26)	Fe–N(2)′	1.872 (24)
	Angles		
Fe–S(1)–Fe	75.7 (2)	Fe–S(1)′–Fe	74.5 (2)
S(1)–Fe–N(1)	109.3 (4)	S(1)′–Fe–N(1)	111.5 (4)
S(1)–Fe–N(2)	107.2 (7)	S(1)′–Fe–N(2)′	109.7 (7)
S(1)–Fe–N(1)	115.7 (4)	S(1)′–Fe–N(1)	112.6 (4)
S(1)–Fe–N(2)	109.3 (7)	S(1)′–Fe–N(2)′	118.1 (7)
N(1)–Fe–N(2)	110.6 (6)	N(1)–Fe–N(2)′	99.5 (7)
S(1)–Fe–S(1)	104.3 (4)	S(1)′–Fe–S(1)′	105.5 (4)

[a] For the cation in $[(C_2H_5)_4N]_2Fe_2S_2(C_4H_4N)_4$, the N–C bonds are within the range 1.464 (23)–1.704 (29) Å with a mean value of 1.541 (29) Å. The C–C bonds are within the range 1.415 (27)–1.599 (31) Å with a mean value of 1.519 (31) Å. The values given above are obtained from all N(C)–C bonds of the two possible orientations of the disordered tetraethylammonium cation.

C–N bond of 1.513 (5) Å and will not be considered further. Selected atomic distances and angles are compiled in Table VI. The core structural details in I are compared to those in II–IV in Table X.

In the crystal structure, the $[Fe_2S_2(o,o'\text{-}C_{12}H_8O_2)_2]^{2-}$ anion (Figure 2) is located on a crystallographic center of inversion ($^3/_4$, $^1/_4$, 0). Two Fe(III) ions with distorted tetrahedral coordination are bridged by two sulfide ions and are terminally coordinated by two phenolate oxygens. The $[Fe_2S^*_2]^{2+}$ core is planar with a Fe–Fe distance of 2.699 (1) Å and a S*–S* distance of 3.512 (2) Å. The Fe--Fe distance is very close to those in $[Fe_2S_2(S_2\text{-}o\text{-xyl})_2]^{2-}$ (Fe--Fe = 2.698 (1) Å)[5] and $[Fe_2S_{12}]^{2-}$ (Fe--Fe = 2.701 (3) Å).[6] The S*–S* distance is slightly longer than those in $[Fe_2S_2(S_2\text{-}o\text{-xyl})_2]^{2-}$ and $[Fe_2S_{12}]^{2-}$ by about 0.01 and 0.06 Å, respectively.

The structure of the core shows two pairs of unequal Fe–S* distances that differ by 0.011 Å. Unequal Fe–S* distances also have been observed in the structure of the *o*-xylyl dimer[5] with a difference of 0.047 Å.

Table VIII. Selected Distances (Å) and Angles (deg) in the Anion[a] of $(Et_4N)_2Fe_2S_2[O\text{-}o\text{-}C_6H_4CH(n\text{-Bu})NHC_6H_4\text{-}o\text{-}S]_2$

	Distances		
Fe(1)–S(2)	2.206 (5)	Fe(1)–S(1)	2.308 (5)
Fe(1)–S(2)	2.198 (5)		
mean	2.202 (5)		
Fe(1)···Fe(1)	2.709 (5)	S(2)···S(2)	3.473 (5)
Fe(1)–O(1)	1.921 (11)		
Fe(1)–N(1)	3.638 (11)		
S(1)–C(1)	1.800 (19)		
O(1)–C(7)	1.368 (19)		
	Angles		
Fe(1)–S(2)–Fe(1)	75.9 (2)	S(2)–Fe(1)–S(2)	104.1 (3)
S(1)–Fe(1)–S(2)	106.6 (2)	S(1)–Fe(1)–S(2)	113.1 (2)
O(1)–Fe(1)–S(2)	114.2 (4)	O(1)–Fe(1)–S(2)	112.6 (4)
O(1)–Fe(1)–S(1)	106.2 (3)		
		Fe(1)–S(1)–C(1)	101.9 (6)
		Fe(1)–O(1)–C(7)	129.6 (1.0)
C(1)–C(2)–N(1)	119.8 (1.9)		
C(2)–N(1)–C(13)	119.6 (1.6)		
C(7)–C(8)–C(13)	121.4 (1.8)		

[a] For the cation in $[(C_2H_5)_4N]_2Fe_2S_2(O\text{-}o\text{-}C_6H_4CH(n\text{-Bu})NHC_6H_4\text{-}o\text{-}S)_2$, the N–C bonds are within the range 1.517 (23)–1.532 (21) Å with a mean value of 1.522 (23) Å. The C–C bonds are within the range 1.516 (25)–1.522 (28) Å with a mean value of 1.518 (28) Å. The six C_i–N–C_j angles are found between 105.9 (1.4) and 112.0 (1.4)° with a mean value of 109.5 (1.4)°. The N–C_i–C_j angles are found between 114.4 (1.6) and 115.0 (1.6)° with a mean value of 114.7 (1.6)°.

Table IX. Selected Distances (Å) and Angles (deg) in the Anion[a] of the $(C_6H_5)_4P^+$ Salt of $Fe_2S_2(OC_6H_4\text{-}p\text{-}CH_3)_4^{2-}$

	Distances		
Fe(1)–S(1)	2.229 (5)	Fe(1)–O(1)	1.879 (11)
Fe(1)–S(1)	2.222 (5)	Fe(1)–O(2)	1.874 (9)
Fe(2)–S(2)	2.219 (5)	Fe(2)–O(3)	1.855 (12)
Fe(2)–S(2)	2.223 (5)	Fe(2)–O(4)	1.872 (11)
mean	2.223 (5)	mean	1.870 (12)
Fe(1)···Fe(1)	2.772 (5)	S(1)···S(1)	3.483 (8)
Fe(2)···Fe(2)	2.725 (5)	S(2)···S(2)	3.508 (9)
mean	2.749 (24)	mean	3.496 (9)
O(1)–C(1)	1.319 (17)		
O(2)–C(7)	1.329 (16)		
O(3)–C(13)	1.335 (17)		
O(4)–C(19)	1.339 (17)		
	Angles		
Fe(1)–S(1)–Fe(1)	77.0 (2)	S(1)–Fe(1)–S(1)	103.0 (3)
Fe(2)–S(2)–Fe(2)	75.7 (2)	S(2)–Fe(2)–S(2)	104.3 (3)
mean	76.4 (7)	mean	103.7 (7)
S(1)–Fe(1)–O(1)	112.3 (4)	S(1)–Fe(1)–O(1)	118.0 (4)
S(1)–Fe(1)–O(2)	116.1 (3)	S(1)–Fe(1)–O(2)	115.1 (3)
S(2)–Fe(2)–O(3)	115.5 (4)	S(2)–Fe(2)–O(3)	109.1 (4)
S(2)–Fe(2)–O(4)	113.8 (4)	S(2)–Fe(2)–O(4)	117.4 (4)
		Fe(1)–O(1)–C(1)	135.1 (1.1)
O(1)–Fe(1)–O(2)	93.1 (5)	Fe(1)–O(2)–C(7)	142.6 (1.1)
O(3)–Fe(2)–O(4)	97.2 (6)	Fe(2)–O(3)–C(13)	130.4 (1.1)
mean	95 (2)	Fe(2)–O(4)–C(19)	133.5 (1.2)

[a] For the cation in $[(C_6H_5)_4P]_2Fe_2S_2(OC_6H_4\text{-}p\text{-}CH_3)_4$ the eight P–C bonds are within the range 1.753 (15)–1.805 (15) Å with a mean value of 1.782 (16) Å. The C–C bonds are within the range 1.312 (27)–1.434 (23) Å with a mean value of 1.385 (28) Å. The twelve C_i–P–C_j angles are found between 107.3 (7) and 112.0 (7)° with a mean value of 109.5 (8)°. The C–C–C angles are in the range 115.0 (2)–124.0 (2)° with a mean value of 120.0 (2)°.

The Fe–S*–Fe angle of 75.1° is greater than the idealized value of 70.5° expected for the interior bridge angle of two perfect tetrahedra sharing a common edge and is comparable to that encountered in $[Fe_2S_{12}]^{2-}$ and $[Fe_2S_2(S_2\text{-}o\text{-xyl})_2]^{2-}$ (76.1 (1) and 75.27 (5)°, respectively). The dihedral angle between the $Fe_2S^*_2$

Table X. Comparison of Selected Structural Parameters for the $[Fe_2S_2L_4]^{2-}$ Anions [L_2 = *o,o'*-$C_{12}H_8O_2^{2-}$ (I), L = $C_4H_4N^-$ (II), L_2 = (O-*o*-C_6H_4CH(*n*-Bu)NHC_6H_4-*o*-S)$^{2-}$ (III), and L = $^-OC_6H_4$-*p*-CH_3 (IV)]

	III[a]	I[a]	IV[a,b]	II[a,c]
Fe–Fe, Å	2.709 (5)	2.699 (1)	2.749 (24)	2.677 (3)
Fe–S_b, Å	2.202 (5)	2.215 (6)	2.223 (5)	2.19 (6)
Fe–O(N), Å	1.921 (11)	1.894 (2)	1.870 (12)	1.97 (5)
Fe–S_t, Å	2.308 (5)			
S_b–S_b, Å	3.473 (5)	3.512 (2)	3.496 (9)	3.48 (4)
S_b–Fe–S_b, deg	104.1 (3)	104.9 (1)	103.7 (7)	104.9 (6)
Fe–S_b–Fe, deg	75.9 (2)	75.1 (1)	76.4 (7)	75.1 (6)

[a] This work. [b] Values reported here are averaged over two fragments in the asymmetric unit. [c] Averaged values of individual bond distances and angles from two possible orientations of the disordered anion.

and FeO(1)O(2) planes is 86.39°, less than the value seen for the *o*-xylyl dimer (89.95°). Further departure of the stereochemistry at the Fe sites from idealized T_d symmetry is evident in bond angle values, which vary from 104.9 (1) (S*–Fe–S*) to 117.8 (1)° (O(2)–Fe–S*). The O(1)–Fe–O(2) angle is 96.1 (1)°.

The two phenyl rings of the coordinated biphenolate ligand are tilted relative to each other with a dihedral angle of 133.1°. The Fe–O distance in I at 1.894 (2) Å is significantly longer than the mean Fe–O distances found in $Fe(OAr)_4^-$[23] (1.847 (7) Å, Ar = 2,3,5,6-$(CH_3)_4C_6H$; 1.866 (3) Å, Ar = 2,4,6-$Cl_3C_6H_2$) and $[Fe_4S_4(OC_6H_5)_4]^{2-}$[25] (1.865 (8) Å); however, it is similar to that in $[Fe_6S_6(OAr)_6]^{3-}$[24] (1.880 (11) Å).

$[(C_2H_5)_4N]_2[Fe_2S_2(C_4H_4N)_4]$ (II). The compound crystallizes in space group $P2_1/n$ of the monoclinic system with two molecules per unit cell. The crystal structure consists of discrete cations and anions. The tetraethylammonium cations are positionally disordered and assume two different orientations. Their structural details are unexceptional and will not be considered further. Selected distances and angles of the anion are compiled in Table VII. The core structural details in II are compared to those in I, III, and IV in Table X.

In the crystal structure, the $[Fe_2S_2(C_4H_4N)_4]^{2-}$ anion (Figure 3) is located on a crystallographic inversion center (0, 0, 0). In the anion, the $[Fe_2S_2^*]$ core and one of the pyrrolate rings are found positionally disordered with approximately 50% occupancy. In both orientations (Figure 1) that the anions can assume, the $[Fe_2S_2^*]$ core is required to be planar with a Fe···Fe distance of 2.677 (3) Å. This distance is shorter than those reported for thiophenolate and phenolate dimers by about 0.02 Å and the shortest among $[Fe_2S_2^*]$ dimers reported to date. The S*--S* distance in the two orientations of the core has values of 3.439 (15) and 3.515 (15) Å, which are comparable to those of the thiophenolate and phenolate dimers.

The Fe–S* distances in the two orientations yield a mean value of 2.19 (6) Å, which falls within the range of Fe–S* distances of the known oxo and thio analogues. In the first orientation, the two Fe–S* distances are 2.275 (8) and 2.078 (8) Å, respectively. In the second orientation, the two Fe–S* distances are 2.316 (8) and 2.096 (8) Å, respectively. It is obvious that, in both orientations of the pyrrolate anion, the individual Fe–S* distances are unusually dissimilar unlike what has been observed in the other dimers characterized so far. The origin of this inequality in the two Fe–S* distances in each orientation of the Fe_2S_2 dimer is difficult to explain. The dihedral angles between the $Fe_2S_2^*$ and FeN(1)N(2) and FeN(1)N(2)′ planes are 88.79 and 87.44°, respectively. The stereochemistry of the Fe sites in the $[Fe_2S_2^*]$ core departs from idealized T_d symmetry with angles that range from 104.3 (4) (S*–Fe–S*) to 118.1 (7)° (S*–Fe–N(2)′). The bond angle values observed here are in the same range as those of the other dimers reported thus far.

In the first orientation of the anion, the two pyrrolate planes define a dihedral angle of 88.8°, whereas in the second orientation this angle is 72.2°.

The Fe–N distances range from 1.87 (2) to 2.09 (3) Å with a mean value of 1.97 (5) Å, which is within 3σ from the corresponding distance of high-spin XFe^{III}–porphyrin complexes (X = Cl^-, SCN^-, N_3^-),[28] $(Fe–N)_{av}$ = 2.07 Å, and the Fe–N distances of high-spin Fe(III) complexes in which the iron is coordinated to nitrogen atoms of multidentate chelating agents. Examples of the latter are Fe(saloph)catH ($Fe–N_{av}$ = 2.097 (5) Å),[29] $[Fe(salen)]_2$hq ($Fe–N_{av}$ = 2.096 (5) Å),[29,31] and $[Fe(salen)]_2O$[30,31] and Fe(salen)Cl ($Fe–N_{av}$ = 2.091 (6) Å).[32]

$[(C_2H_5)_4N]_2[Fe_2S_2$(O-*o*-C_6H_4CH(*n*-Bu)NHC_6H_4-*o*-S)$_2$] (III). The compound crystallizes in space group $P2_1/c$ of the monoclinic system with two molecules per unit cell. The crystal structure consists of discrete cations and anions. The tetraethylammonium cations have their expected unexceptional geometry with a mean C_i–N–C_j angle of 109.5 (1.4)° and a mean C–N bond length of 1.522 (23) Å and will not be considered further. Atomic distances and angles are compiled in Table VIII.

In the crystal structure, the anion (Figure 4) is located on a center of inversion ($^1/_2$, $^1/_2$, $^1/_2$). Structural features within the centrosymmetric $Fe_2S_2^*$ rhombic unit are comparable to those in I, II, and IV (Table X). The dihedral angle between the two phenyl rings in the ligand is 89.37°.

The nitrogen atom of the chelate ligand is located 1.39 (2) Å from atom C(2) of the phenyl ring attached to sulfur and 1.46 (2) Å from the chiral carbon atom C(13). The conformation adopted by the bidentate chelate mixed ligand in the crystal structure has the nitrogen atom situated away from the iron atom of the $[Fe_2S_2^*]$ core at a nonbonding distance of 3.638 (11) Å. Previous reports in the literature cite the presently employed mixed donor atom ligand as a potential tridentate ligand in complexes that involve first-row transition metals.[27d] An examination of molecular models shows that the ligand in III could assume a tridentate mode of coordination to the iron. Whether this can take place in the one-electron-reduced complex is at present under study in our laboratory. To date, there exist no crystallographically determined complexes that contain the $[Fe_2S_2^*]^{2+}$ core with five-coordinate iron atom(s).

$[(C_6H_5)_4P]_2[Fe_2S_2(OC_6H_4$-*p*-$CH_3)_4]$ (IV). The compound crystallizes in space group $P2_1/a$ of the monoclinic system with four molecules per unit cell. The crystal structure consists of discrete cations and anions. The structures of the $(C_6H_5)_4P^+$ cations are unexceptional and will not be considered further. Selected distances and angles of the anion are compiled in Table IX. Selected structural parameters for IV are compared to those in I, II, and III in Table X.

In the crystal structure of $[(C_6H_5)_4P]_2Fe_2S_2[(OC_6H_4$-*p*-$CH_3)_4]$, the anions (Figure 5) are sitting on crystallographic inversion centers, and in the asymmetric unit there are two half-anions (A and B) and two tetraphenyl phosphonium cations. The inversion centers on which the two anions are located are ($^1/_2$, $^1/_2$, $^1/_2$) and (0, $^1/_2$, 0). The $[Fe_2S_2^*]$ cores in both anions are required by symmetry to be planar and show Fe···Fe distances of 2.772 (5) and 2.725 (5) Å. These Fe···Fe distances are significantly longer than those observed in I (2.699 (1) Å) (Table X). They are also longer than the Fe···Fe distances observed in the thiolate analogue by 0.081 and 0.034 Å, respectively. The distance between the bridging sulfur atoms S*···S* in the first $[Fe_2S_2^*]$ core (anion A) is 3.483 (8) Å, identical, within experimental uncertainty, with that found in the thiolate analogue whereas the S*···S* distance in the second $[Fe_2S_2^*]$ core (anion B) is 3.508 (9) Å, slightly longer than that in the thiolate analogue[5] and very similar to that observed in I (3.512 (2) Å).

Departure of the stereochemistry at the Fe sites from idealized

(28) Scheidt, W. R. In *The Porphyrins*; Dolphin, D., Ed.; Academic: New York, 1978; Vol. III, Chapter 10 and references therein.
(29) Heistand, R. H., II; Roe, A. L.; Que, L., Jr. *Inorg. Chem.* **1982**, *21*, 676.
(30) (a) Gerloch, M.; McKenzie, E. D.; Towl, A. D. C. *J. Chem. Soc. A* **1969**, 2850. (b) Coggon, P.; McPhail, A. T.; Mabbs, F. E.; McLachlan, V. N. *J. Chem. Soc. A* **1971**, 1014.
(31) Abbreviations used: Fe(saloph)catH, [*N,N'*-(1,2-phenylene)bis(salicylideneaminato)](catecholato-*O*)iron(III); [Fe(salen)]$_2$hq, (μ-1,4-benzenediolato-*O,O'*)bis[*N,N'*-ethylenebis(salicylideneaminato)iron(III)]; [Fe(salen)]$_2$O, (μ-oxo)bis[*N,N'*-ethylenebis(salicylideneaminato)iron(III)]; Fe(salen)Cl, [*N,N'*-ethylenebis(salicylideneaminato)]iron(III) chloride.
(32) Gerloch, M.; Mabbs, F. E. *J. Chem. Soc. A* **1967**, 1598.

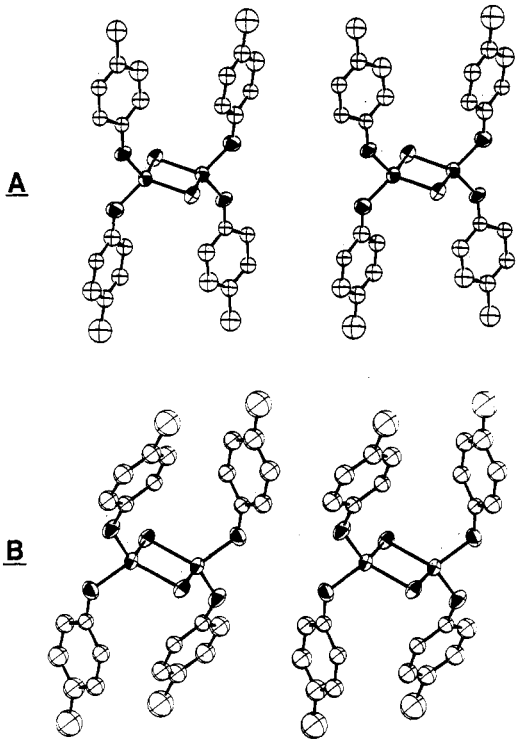

Figure 6. (a) Perspective view of the $[Fe_2S_2(OC_6H_4\text{-}p\text{-}CH_3)_4]^{2-}$ anion (A) as drawn by ORTEP. (b) Perspective view of the $[Fe_2S_2(OC_6H_4\text{-}p\text{-}CH_3)_4]^{2-}$ anion (B) as drawn by ORTEP.

T_d symmetry is evident from bond angle values, which vary from 103.0 (3)° (S*–Fe–S*) to 118.0 (4)° (O(1)–Fe–S*) in both anions. The range of bond angle values observed here is similar to that observed for I.

The O(1)···O(2) and O(3)···O(4) distances in the two anions are shorter than the S_t···S_t distance in the thiolate analogue by approximately 1 Å.

In anion A the tolyl rings make an angle of 17.6° with each other. An examination of the spatial disposition of the tolyl rings in the Fe–O–Ar units of the $[Fe_2S_2^*]^{2+}$ core reveals that the $FeOC_6H_4\text{-}p\text{-}CH_3$ units are not planar and the tolyl rings appear to have rotated about the O–C bonds by 3.3 and 32.2°. In anion B, the tolyl rings are oriented at a dihedral angle of 79.2° relative to each other. Here, also, the Fe–O–Ar units are not planar. In one of the $FeOC_6H_4\text{-}p\text{-}CH_3$ units, the tolyl ring has rotated about the C–O bond by 19.1° whereas in the other the rotation angle of the tolyl ring about the C–O bond is 36.6°.

It is apparent that in both anions of $[Fe_2S_2(OC_6H_4\text{-}p\text{-}CH_3)_4]^{2-}$, the orientation of the phenyl ring in the $OC_6H_4\text{-}p\text{-}CH_3$ unit is not the one parallel to the Fe–O bond. The parallel orientation of the phenyl rings is the preferred one in the case of $[Fe(SPh)_4]^{2-}$, and the distortions arising from that have been described in detail.[33] Similar preference for the parallel mode of binding is also observed with the $CH_3\text{-}p\text{-}C_6H_4S^-$ ligand in the structure of the $[Fe_2S_2(SC_6H_4\text{-}p\text{-}CH_3)_4]^{2-}$ complex.

In the phenoxide dimer, only one of the $FeOC_6H_4\text{-}p\text{-}CH_3$ units is close to being planar (rotation angle 3.3°). This lack of planarity can be rationalized if one considers that the short Fe–O bonds would result in unacceptably short Fe–ortho hydrogen and S–ortho hydrogen contacts in both anions. As a result the tolyl rings twist out of the M–O–C plane. In the present relaxed configuration the closest ortho hydrogen–Fe and ortho hydrogen–S contacts are 3.229 and 3.272 Å for anion A and 3.176 and 3.316 Å for anion B. Similar behavior is observed in the structure of the $C(SC_6H_5)_4$[34] molecule (C–S = 1.826 Å) where the phenyl rings are twisted toward an approximate orthogonal orientation relative to the C–S bonds. In $[Fe_2S_2(OC_6H_4\text{-}p\text{-}CH_3)_4]^{2-}$ the Fe–O–C angles for both anions vary from 130.4 (1.1) to 142.6 (1.1)°. Perspective views of the two anions (A and B) are given in Figure 6.

The Fe–O distance in the two anions ranges from 1.855 (12) to 1.879 (11) Å with a mean of 1.877 (11) Å for anion A and 1.864 (12) Å for anion B. These values are slightly shorter than that of the biphenolate analogue and compares fairly well with values reported for the phenolate cubane[25] and the cresolate prismane[24] clusters.

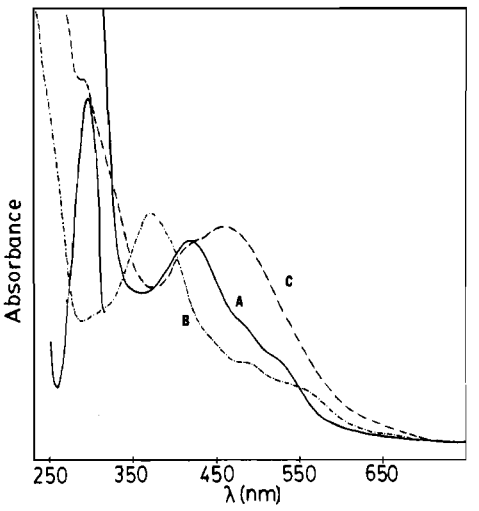

Figure 7. Electronic spectra of the $[Fe_2S_2(o,o'\text{-}C_{12}H_8O_2)_2]^{2-}$ (A, —), $[Fe_2S_2(C_4H_4N)_4]^{2-}$ (B, –·–), and $[Fe_2S_2(O\text{-}o\text{-}C_6H_4CH(n\text{-}Bu)NHC_6H_4\text{-}o\text{-}S)_2]^{2-}$ (C, - - -) anions.

Electronic Spectra. The electronic spectra of I–IV (Figure 7) resemble those of the Fe_2S_2 complexes with sulfur donor terminal ligands. The low-energy electronic absorptions in the $[Fe_2S_2(SAr)_4]^{2-}$[35] and $[Fe_2S_2X_4]^{2-}$ complexes, (X = Cl^-, Br^-, I^-)[19] have been assigned previously to terminal ligand-to-metal charge-transfer transitions. Similar assignments have been made for $[Fe_4S_4(OAr)_4]^{2-}$[25] (410 nm, Ar = Ph; 424 nm, Ar = $-C_6H_4\text{-}p\text{-}CH_3$) and for [Fe(2,3,5,6-tetramethylphenolate)$_4$]$^-$ (422 nm[23]).

The hypsochromic shift observed (~80 nm) upon substitution of sulfur by oxygen has been encountered before in the $[Fe_4S_4(OAr)_4]^{2-}$ and $[Fe_6S_6(OAr)_6]^{3-}$ clusters. Spectral comparisons between dimers and tetramers as well as comments on the effect of aryl substituents on the energies of these absorptions have been made previously.[16] A qualitative comparison of the electronic spectra of the phenoxy and pyrrolate dimers to the spectrum of the oxidized Rieske protein from *Thermus thermophilus*[12] (λ_{max} (nm) (ϵ_m): 325 (11 500), 458 (6000), 560 (sh ~ 3000) reveals a considerable degree of similarity among all three, although the spectra of the synthetic dimers are blue-shifted relative to that of the Rieske protein.

The spectrum of III in CH_3CN solution exhibits a broad absorption maximum in the 400–470-nm region. The band is preceded by a shoulder in the same region. The spectrum is qualitatively similar to the spectra of the aryloxide $[Fe_2S_2L_4]^{2-}$ (L = $^-OC_6H_4CH_3$, L_2 = $o,o'\text{-}C_{12}H_8O_2^{2-}$) and $[Fe_2S_2(SAr)_4]^{2-}$ (Ar = $^-SC_6H_4\text{-}p\text{-}CH_3$, $^-SC_6H_5$)[35] dimers. The shoulder around 414 nm is of similar energy to absorptions found in the aryloxide Fe_2S_2 dimers, whereas the absorption maximum at 457 nm is close in energy to absorptions observed with the thiolate dimers. The possibility that III exists in solution in equilibrium with other isomers (vide infra) was considered, and the electronic spectra were obtained in solvents with different dielectric properties.

A change in the solvent from CH_3CN to DMF does not dramatically affect the appearance of the spectrum. The ligand-to-metal charge-transfer absorptions are still present in the 400–470-nm region. The relative intensities of the two absorptions, however, have changed. The shoulder around 414 nm (CH_3CN)

(33) Coucouvanis, D.; Swenson, D.; Baenziger, N. C.; Murphy, C.; Holah, D. G.; Sfarnas, N.; Simopoulos, A.; Kostikas, A. *J. Am. Chem. Soc.* **1981**, *103*, 3351.

(34) Kato, V. *Acta Crystallogr., Sect. B: Struct. Crystallogr. Cryst. Chem.* **1972**, *B28*, 606.

(35) Reynolds, J. G.; Holm, R. H. *Inorg. Chem.* **1980**, *19*, 3257.

Table XI. Observed Chemical Shifts, $(\Delta H/H_0)_{obsd}$ (ppm), for the Complexes and Appropriate Diamagnetic References,[a] $(\Delta H/H_0)_{diam}$

	chem shift					
	o-H	*m*-H	*p*-H	N–H	*m*-CH_3	*p*-CH_3
$(Et_4N)_2Fe_2S_2(o,o'\text{-}C_{12}H_8O_2)_2$[b]	2.73	9.27, 9.61	2.14			
$(Ph_4P)_2Fe_2S_2(OC_6H_4\text{-}p\text{-}CH_3)_4$[b]	2.51	10.76				6.78
$(Ph_4P)_2Fe_2S_2(OC_6H_4\text{-}m\text{-}CH_3)_4$[b]	2.63	10.72	2.14		0.76	
$(Et_4N)_2Fe_2S_2(SC_6H_4\text{-}p\text{-}CH_3)_4$[c]	4.68	9.20				6.02
$(Et_4N)_2[Fe_2S_2(O\text{-}o\text{-}C_6H_4CH(n\text{-}Bu)NHC_6H_4\text{-}o\text{-}S)_2]$[b]		11.02, 10.23[d]		3.87		
		(11.20)[e]		(4.00)[e]		
		8.70, 8.33[f]	5.40			
		(8.83, 8.19)[e]	(5.48)[e]			
$(Et_4N)_2Fe_2S_2(C_4H_4N)_4$[b]	10.25	8.92				
$p\text{-}CH_3C_6H_4OH$	6.80	6.80				2.25
$o,o'\text{-}C_{12}H_{10}O_2$	7.03	7.03	7.03			
C_4H_5N	6.79 (α-H)	6.18 (β-H)				
$m\text{-}CH_3C_6H_4OH$	6.55	6.55	6.55		1.91	
$C_{13}H_{11}NOS$[g]	6.95	6.95	6.95	5.45		

[a] The isotropic shifts, $(\Delta H/H_0)_{iso}$ are defined as $(\Delta H/H_0)_{diam} - (\Delta H/H_0)_{obsd} = (\Delta H/H_0)_{iso}$. [b] Measured in CD_3CN at room temperature. [c] From ref 35. [d] Resonances associated with the *O*-phenyl ring. [e] A micro component tentatively attributed to another isomer or conformer. [f] Resonances associated with the *S*-phenyl ring. [g] The C–H proton is found at 2.17 ppm.

has emerged as a band at 410 nm whereas the band at 457 nm (CH_3CN) has faded into a shoulder around 460 nm. These observations, together with ^1H NMR data (vide infra) suggest that other isomers of III may indeed be present in solution.

^1H NMR Spectroscopy and Solution Magnetic Studies. The ^1H nuclear magnetic resonance spectra (NMR) of the $[L_2FeS_2FeL_2]^{2-}$ dimers, I–IV were measured in deuteriated acetonitrile solutions. Isotropic shifts of the aromatic ring protons are given in Table XI. Representative 300- and 360-MHz ^1H NMR spectra of these complexes are shown in Figure 8.

The patterns of the isotropically shifted resonances in I and III are similar to those in the spectra of $[Fe_2S_2(SAr)_4]^{2-}$,[35] $[Fe_4S_4(XAr)_4]^{2-}$ (X = O, S),[25,36] and $[Fe_6S_6(XAr)_6]^{3-}$ (X = O, S).[24] The isotropic shifts of the phenyl ring resonances of the phenoxy dimers are clearly greater in magnitude than those of the corresponding resonances of the arenethiolate dimers. This suggests a more efficient propagation of unpaired electron spin density through the Fe–O–C bonds[25,36] and implies a relatively more covalent Fe–O bond.

The pattern of alternating signs of the isotropic shifts has been observed before in the thiolate dimers, cubane tetramers, and prismane hexamers and has been attributed[36] to dominant Fermi contact interactions (π-delocalization mechanism) with negligible dipolar contributions. The ortho hydrogen signals in all complexes are identified by the relative broadness due to relaxation effects induced by their proximity to the paramagnetic center. The shifts of the *p*-CH_3 resonance to low fields is consistent with the assumption that π-electron spin density at the para position leads to a direct contact interaction with the methyl group protons via hyperconjugation.[36,37]

The α-H and β-H proton signals in the $[Fe_2S_2(C_4H_4N)_4]^{2-}$ dimer show isotropic shifts of the same sign. Although this behavior suggests that the shifts are due primarily to contact interactions with the spin transfer taking place through a direct σ-delocalization mechanism, partial electron spin density transfer through π bonds within the aromatic pyrrolate ring is still possible.

In the mixed-ligand oxo–thio dimer III there are two sets of meta protons (each set consisting of two protons), which appear at low fields (compared to the diamagnetic ligand). Both sets of meta protons are accompanied by minor peaks with resonances very close to those of the major ones. It is assumed that these minor peaks are due to the presence of a different structural or conformational isomer of III that in solution coexists with the trans isomer found in the solid-state structure.

The spectrum of the mixed-ligand dimer in deuteriated dimethylformamide shows the same pattern of isotropically shifted resonances for the phenyl ring protons as in deuteriated CH_3CN.

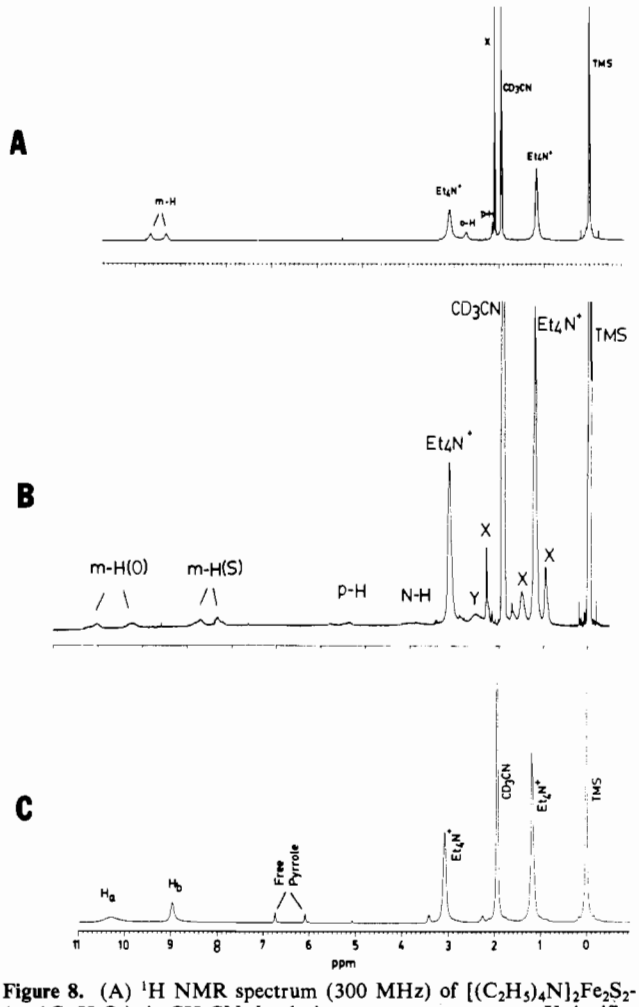

Figure 8. (A) ^1H NMR spectrum (300 MHz) of $[(C_2H_5)_4N]_2Fe_2S_2(o,o'\text{-}C_{12}H_8O_2)_2$ in $CH_3CN\text{-}d_3$ solution at room temperature. X signifies an unattributed signal. (B) ^1H NMR spectrum (300 MHz) of $[(C_2H_5)_4N]_2Fe_2S_2[O\text{-}o\text{-}C_6H_4CH(n\text{-}Bu)NHC_6H_4\text{-}o\text{-}S]_2$ in $CH_3CN\text{-}d_3$ solution at room temperature. X indicates *n*-Bu signals. Y signifies an unattributed signal. (C) ^1H NMR spectrum (360 MHz) of $[(C_2H_5)_4N]_2Fe_2S_2(C_4H_4N)_4$ in $CH_3CN\text{-}d_3$ solution at room temperature.

The isotropic shifts of the phenyl (aryl) protons of the phenoxy dimers show temperature dependence. The magnitude of the isotropic shifts in I, II, and IV increases linearly with increasing temperature over the temperature range of −30 to +60 °C. This result is consistent with the existence of intramolecular antiferromagnetic coupling in the dimers and is similar to the magnetic

(36) (a) Holm, R. H.; Philips, W. D.; Averill, B. A.; Mayerle, J. J.; Herskovitz, T. *J. Am. Chem. Soc.* **1974**, *96*, 2109. (b) Reynolds, J. G.; Laskowski, E. J.; Holm, R. H. *J. Am. Chem. Soc.* **1978**, *100*, 5315.
(37) Que, L., Jr.; Bobrik, M. A.; Ibers, J. A.; Holm, R. H. *J. Am. Chem. Soc.* **1974**, *96*, 4168.

Table XII. Cyclic Voltammetric[a] Data for the Et_4N^+ Salts of the $(L_2FeS_2FeL_2)^{2-}$ Clusters [L_2 = $C_{12}H_8O_2^{2-}$ (I), L = $C_4H_4N^-$ (II), L_2 = ^-O-*o*-C_6H_4CH(*n*-Bu)NHC_6H_4-*o*-S^- (III), L = $C_6H_5S^-$, Cl^-]

compd	E_p,[b] V (of 2−/3− couple)	compd	E_p,[b] V (of 2−/3− couple)
		CH_3CN	
I	−1.52	$(Et_4N)_2Fe_2S_2Cl_4$[c]	−1.00
II	−1.44	$(Et_4N)_2Fe_2S_2(SC_6H_5)_4$	−1.25
III	−1.47		
		DMF	
I	−1.45	$(Et_4N)_2Fe_2S_2Cl_4$	−1.09
II	−1.28	$(Et_4N)_2Fe_2S_2(SC_6H_5)_4$	−1.20
		CH_2Cl_2	
I	−1.41	$(Et_4N)_2Fe_2S_2Cl_4$	−1.01
II	−1.26	$(Et_4N)_2Fe_2S_2(SC_6H_5)_4$	−1.17
III	−1.32		

[a] The supporting electrolyte was *n*-Bu_4NClO_4, 0.1 M. For all measurements, the scan rate was 200 mV/s. Potentials are vs SCE. [b] All waves are irreversible. [c] It was recorded at 100 mV/s.

behavior of the well-characterized $[Fe_2S_2(S_2$-*o*-xyl$)_2]^{2-}$ and $[Fe_2S_2Cl_4]^{2-}$ dimers. The magnetic susceptibilities of I, II, and IV were measured by the ^1H NMR Evans method in CD_3CN solution at 298 K. The magnetic moments (μ_{eff}^{cor}/Fe) are 1.46, 1.52, and 1.86 μ_B, respectively. These values are comparable to those reported for $[Fe_2S_2Cl_4]^{2-}$ (μ_{eff}^{cor}/Fe = 1.38 μ_B) and $[Fe_2S_2(S_2$-*o*-xyl$)_2]^{2-}$ (μ_{eff}^{cor}/Fe = 1.43 μ_B) and reaffirm the presence of antiferromagnetically coupled irons in the dimeric complexes.

Electrochemical Measurements. The electrochemical behavior of I–III was studied by cyclic voltammetry in CH_3CN, DMF, and CH_2Cl_2 solutions. For comparison, the clusters $[Fe_2S_2Cl_4]^{2-}$ (L = Cl^-, $SC_6H_5^-$) were examined under identical conditions. The electrochemical results are summarized in Table XII.

The data show that the 2−/3− reductions of I–III occur at more negative potentials than those of the halide and arenethiolate analogues. The cyclic voltammetric waves of the 2−/3− redox couples are indicative of irreversible or quasi-reversible processes. Similar electrochemical behavior has been previously observed for the $[Fe_2S_2(SC_6H_5)_4]^{2-}$ [35,38] and $[Fe_2S_2Cl_4]^{2-}$ [19] clusters.

Mössbauer Spectra. The Mössbauer spectra of I–III were recorded (in the solid state at 77 K and zero applied field). Also recorded for comparison purposes under the same conditions were the Mössbauer spectra of $[Fe_2S_2Cl_4]^{2-}$ and $[Fe_2S_2(SPh)_4]^{2-}$ [39] dimers (Table XIII). Isomer shifts are given relative to Fe metal at room temperature. The spectra in the solid state consist of single, sharp quadrupole doublets, and the reported hyperfine parameters were obtained by fitting the data for each of the complexes with two Lorentzian lines. Examination of the data shows that the trend in the isomer shift values as a function of the terminal ligand donor atom (S vs O) parallels similar trends in the corresponding cubane and prismane clusters. The narrow range of isomer shift values (range: 0.26–0.37 mm/s) shows that these parameters are rather insensitive to the nature of the terminal ligands. It is not surprising therefore that the isomer shift and the quadrupole splitting values of I–III are similar to those reported for the oxidized Rieske protein from *T. thermophilus*[12] (Table XIII) and spinach Fd(ox)[40] (IS = 0.26 mm/s, ΔE_q = 0.65 mm/s). The frozen CH_3CN solution spectrum of III ($C = 0.9 \times 10^{-2}$ M) was fitted with four lines, assuming the same width at half-maximum as that used in the fit of the solid-state spectrum. The broadening apparent in the frozen-solution spectrum of III is significant, and it may arise from the presence of more than one isomer. This possibility also finds support in the complexity of the ^1H NMR spectrum in CD_3CN solution.

Table XIII. Isomer Shifts[a] and Quadrupole Splittings of $[L_2FeS_2FeL_2]^{2-}$ Dimers

compd	T, K	δ, mm/s	ΔE_q, mm/s
I	77	0.35 (2)	1.02 (1)
$[(C_2H_5)_4N]_2Fe_2S_2(OC_6H_5)_4$[b]	4.2	0.37	0.32
$[(C_2H_5)_4N]_2Fe_2S_2(SC_6H_5)_4$	77	0.29 (1)	0.33 (1)
$[(C_2H_5)_4N]_2Fe_2S_2(S_2$-*o*-xyl$)_2$[c]	4.2	0.28 (3)	0.36 (5)
II	77	0.26 (1)	0.49 (1)
III	125	0.31 (2)[d,e]	0.45 (2)
		0.31 (2)[e,f]	0.51 (2)
Rieske protein (ox)[g]	4.2	0.32 (1)	0.91 (2)
		0.24 (1)	0.52 (2)

[a] With respect to Fe metal at room temperature. [b] From ref 16. [c] From ref 39. [d] In the solid state. [e] Isomer shift shown as corrected by second-order relativistic Doppler shift[41] of the absorber. [f] In frozen CH_3CN solution. [g] From ref 12.

Summary and Conclusions

The available spectroscopic data[14] and structural information derived from Fe–EXAFS analysis[15] define the terminal ligand environment of the Fe_2S_2 center in the Rieske proteins. This environment is asymmetric with two cysteinyl sulfur atoms bound to one of the two irons and two light atoms coordinated to the other iron atom. ENDOR studies[13] indicate that at least one of the light atoms is nitrogen. A structurally acceptable synthetic analogue must possess two sulfur ligands asymmetrically disposed with respect to the Fe_2S_2 core, a N donor ligand, and other light-atom donor ligands (N, O).

With the exception of $[Fe_2S_2Cl_4]^{2-}$ the new complexes (I–III) are the only other structurally characterized dimers that contain the Fe_2S_2 cores coordinated fully or partially by non-sulfur terminal ligands. The centrosymmetric disposition of the terminal ligands in these complexes is at variance with the proposed asymmetry in the Rieske centers. Nevertheless, an evaluation of the spectroscopic characteristics and reduction potentials of I–III leads to certain conclusions that should be useful in the future design of more acceptable analogues.

The Mössbauer parameters in I–III, by comparison to those of other synthetic analogues with a full complement of sulfur terminal ligands (Table XIII) or to those of biologically occurring Fe_2S_2 centers, are quite similar. This lack of diagnostic sensitivity precludes the application of Mossbauer spectroscopy in the unequivocal detection of different *anionic*, *monodentate* terminal ligands in the Fe_2S_2 cores. The coordination geometry around each of the iron atoms in the Rieske centers is not firmly established. The ability to resolve two quadrupole doublets in the Mössbauer spectra of both the oxidized and the reduced form of the centers is due mainly to different quadrupole splittings for the two iron sites. This difference in electric field gradients could arise from either drastically different terminal ligand environment (neutral ligands?) for the two iron atoms or even a difference in coordination number for one of the iron atoms.

The N donor in the potentially tridentate (O-*o*-C_6H_4CH(*n*-Bu)NHC_6H_4-*o*-S)$^{2-}$ ligand in III (at a distance of 3.64 Å from the iron) is not coordinated (Figure 4). It remains to be seen whether in the reduced form of III the N atom is involved in coordination and a localization of valence occurs as a result of a change in the coordination number for one of the iron atoms. An examination of a molecular model of this ligand shows that, metrically, it also can span the Fe_2S_2 rhombic unit and bind to the two different iron atoms without significant strain. It appears, therefore, that an additional set of cis and trans isomers are possible in solution with the ligands coordinated in an intracore bridging mode. The cis isomer in the latter set will contain $Fe(S)_4$ and $Fe(S)_2(O)_2$ sites. The ^1H NMR spectra of III indicate the presence of other isomers in solution. At present, we are pursuing the isolation and characterization of these isomers.

(38) Cambray, J.; Lane, R. W.; Wedd, A. G.; Johnson, R. W.; Holm, R. H. *Inorg. Chem.* **1977**, *16*, 2565.
(39) Gillum, W. O.; Frankel, R. B.; Foner, S.; Holm, R. H. *Inorg. Chem.* **1976**, *15*, 1095.
(40) (a) Laskowski, E. J.; Frankel, R. B.; Gillum, W. O.; Papaefthymiou, G. C.; Renaud, J.; Ibers, J. A.; Holm, R. H. *J. Am. Chem. Soc.* **1978**, *100*, 5322. (b) Cammack, R.; Dickson, D. P. E.; Johnson, C. E. In *Iron Sulfur Proteins*; Lovenberg, W., Ed.; Academic: New York, 1977; Vol. III, Chapter 8. (c) Dunham, R. W.; Bearden, A. J.; Salmeen, I. T.; Palmer, G.; Sands, R. H.; Orme-Johnson, W. H.; Beinert, H. *Biochim. Biophys. Acta* **1971**, *253*, 134.

The reduction potentials of I-III (Table XII) are considerably more negative than those expected for a Rieske center analogue. Furthermore, they are even more negative than those found for the conventional 2Fe-2S ferredoxin analogues.

Direct comparisons of redox potentials between synthetic analogues and proteins are difficult to make. Potentials for the proteins are obtained in aqueous media and are reported vs the saturated hydrogen electrode (SHE). In contrast, the potentials for the synthetic analogues are obtained in organic solvents (CH_3CN, DMF, etc.) and are reported vs the saturated calomel electrode (SCE). Under the conditions described above regarding solvent and reference electrode, the redox potentials as reported for the most acceptable synthetic analogues (in DMF vs SCE) are more negative by about 1 V than those of the protein centers. Thus, the reduction of the $[Fe_2S_2(SEt)_4]^{2-}$ complex is found at -1.44 V (DMF vs SCE), while the reduction of the 2Fe-2S ferredoxins takes place at around -0.4 V (H_2O vs SHE). The midpoint redox potentials for the Rieske protein from *Thermus thermophilus*[13] and *Pseudomonas putida*[42] are found at +0.15 and -0.11 V, respectively (vs SHE). An acceptable synthetic analogue for the Rieske centers probably should undergo reduction between -0.9 and -1.1 V (in DMF vs SCE). The pH dependence of the midpoint potential in the Rieske protein from *T. thermophilus* has led[43] to the suggestion of the following equilibria:

$$[Fe_2S_2]^{2+},LH + e^- \rightarrow [Fe_2S_2]^{+},LH \text{ at pH } <8$$

$$[Fe_2S_2]^{2+},L^- + e^- + H^+ \rightarrow [Fe_2S_2]^{+},LH \text{ at pH } >8$$

and the proposal that LH is probably coordinated imidazole.

Cognizant of these results, we are currently directing our attention to the synthesis and structural characterization of Fe_2S_2 complexes that contain bidentate ligands that contain OH^- or SH^- and imidazole as functional groups.

Acknowledgment. The support of this work by a grant (GM 26671) from the National Institutes of Health is gratefully acknowledged.

Supplementary Material Available: Tables of fractional atomic coordinates and thermal parameters, hydrogen atom coordinates, anisotropic thermal parameters, and selected bond distances and angles and figures showing edge-on views of the two anions in $[Ph_4P]_2Fe_2S_2(OC_6H_4$-*p*-$CH_3)_4$ and temperature dependences of isotropic shifts (19 pages); tables of observed and calculated structure factors (35 pages). Ordering information is given on any current masthead page.

(41) Dunham, W. R.; Wu, C. T.; Polichar, R. M.; Sands, R. H. *Nucl. Instrum. Methods* **1977**, *145*, 537.
(42) Geary, P. J.; Saboowalla, F.; Patil, D.; Cammack, R. *Biochem. J.* **1984**, *217*, 667.
(43) Kuila, D.; Fee, J. A. *J. Biol. Chem.* **1986**, *261*, 2768.

Contribution from the Department of Chemistry, University of Wisconsin—Milwaukee, Milwaukee, Wisconsin 53201

GC-MS and ^{17}O NMR Tracer Studies of Et_3PO Formation from Auranofin and $H_2{}^{17}O$ in the Presence of Bovine Serum Albumin: An in Vitro Model for Auranofin Metabolism

Anvarhusein A. Isab,[1] C. Frank Shaw III,* and James Locke

Received June 1, 1988

^{17}O NMR spectroscopy and gas chromatographic-mass spectral analysis have been used to monitor the source of oxygen in the triethylphosphine oxide formed by the reaction of the antiarthritic drug auranofin ((2,3,4,6-tetra-*O*-acetyl-β-D-1-glucopyranosato)(triethylphosphine)gold(I)) and bovine serum albumin (BSA) in the presence of reduced glutathione (GtSH). A procedure to extract Et_3PO from aqueous solutions and concentrate it for subsequent analyses was developed. When the in vitro reaction is carried out aerobically in ^{17}O-enriched water, $Et_3P^{17}O$ is generated. The chemical ionization (CH_4) mass measurement, $(m + 1)/z = 135$, and the ^{17}O NMR parameters ($\delta_O = 40.6$ and $^1J_{PO} = 156 \pm 5$ Hz) unambiguously establish its identity. The SH titer of the albumin (mole ratio of protein SH groups to BSA) increases during the reaction, confirming that albumin disulfide bonds are reduced in the reaction. Under aerobic conditions, the enriched Et_3PO accounts for at least 60% of the Et_3PO formed. The significance of these results for the in vivo formation of Et_3PO, an auranofin metabolite, is discussed.

Auranofin ((2,3,4,6-tetra-*O*-acetyl-β-D-1-glucopyranosato)-(triethylphosphine)gold(I), $Et_3PAuSAtg$),[2] a newly licensed chrysotherapy agent, undergoes ligand-exchange reactions that render its metabolism different from that of organic drugs. The products of its metabolic reactions in vivo and model reactions in vitro have been characterized by a variety of physicochemical techniques including radiotracering,[3] ^{31}P NMR,[4,5] ^1H NMR,[5] and EXAFS and XANES spectroscopies,[6] and HPLC.[7] Et_3PO is the principal, and probably exclusive, metabolite generated from the phosphine ligand after it is displaced from the gold(I).[3,5,6,8-10]

Sadler proposed that disulfide bonds in serum albumin oxidize triethylphosphine when $[Au(PEt_3)_2^+]$ is added to whole blood.[5] In packed red blood cells pretreated with auranofin, Et_3PO formation is stimulated by the addition of 2,3-dimercaptopropanol.[5] In reactions of serum albumin with auranofin analogues, auranofin generated a small amount of Et_3PO, but none was generated by

(1) On sabbatical leave for the 1986-1987 academic year from the Department of Chemistry, The King Fahd University of Petroleum and Minerals, Dhahran 31261, Saudi Arabia.
(2) Sutton, B. M. *ACS Symp. Ser.* **1983**, *No. 209*, 371-385.
(3) Intoccia, A. P.; Flanagan, T. L.; Walz, D. T.; Gutzait, L.; Swagzdis, J. E.; Flagiello, J., Jr.; Hwand, B. Y.-H.; Dewey, R. H.; Noguchi, H. In *Bioinorganic Chemistry of Gold Coordination Compounds*; Sutton, B. M., Eds.; Smith Kline and French Laboratories: Philadelphia, PA, 1983; pp 21-33.
(4) Malik, N. A.; Otiko, G.; Sadler, P. J. *J. Inorg. Biochem.* **1980**, *12*, 317-322.
(5) Razi, M. T.; Otiko, G.; Sadler, P. J. *ACS Symp. Ser.* **1983**, *No. 209*, 371-384.
(6) Coffer, M. T.; Shaw, C. F., III; Eidsness, M. K.; Watkins, J. W.; Elder, R. C. *Inorg. Chem.* **1986**, *25*, 333-340.
(7) Tepperman, K.; Finer, R.; Donovan, S.; Elder, R. C.; Doi, J.; Ratliff, D.; Ng, K. *Science (Washington, D.C.)* **1984**, *225*, 430-432.
(8) Dent, J.; Hwang, B., Smith Kline and French Laboratories, personal communication.
(9) Carlock, M. T. M.S. Thesis, University of Wisconsin—Milwaukee, 1985.
(10) Coffer, M. T.; Shaw, C. F., III; Hormann, A. L.; Mirabelli, C. K.; Crooke, S. T. J. *Inorg. Biochem.* **1987**, *30*, 177-187.

0020-1669/88/1327-3406$01.50/0